

## 3.6 Antiproton Tuneshift in the TEVATRON

In the Tevatron, the antiproton bunches suffer a tuneshift due to their interactions with the more intense proton bunches. In multibunch operation, the tuneshifts vary from antiproton bunch to antiproton bunch, leading to an effective spread in tune. An electron lens, consisting of a short, low energy, electron beam propagating along the axis of a solenoidal field, can induce a tuneshift on the antiproton bunches, which has the opposite sign to that, which they experience, from the protons. With appropriate choice of parameters two such lenses could provide effective beam-beam tuneshift compensation. An R&D program has resulted in the construction and, recently, the successful testing of a single such device. If results continue to be positive the use of such devices could lead to a longer luminosity lifetime in the Tevatron and hence to a large integrated luminosity. Further luminosity improvement could come from compensation of the nonlinear beam-beam tune spread using shaped electron beams.

### 3.6.1 Goal and Potential of Beam-Beam Compensation

#### 3.6.1.1 Luminosity of the Tevatron and Beam-Beam Effects in Run II

##### 3.6.1.1.1 Luminosity

As already discussed in Section 2 the luminosity of the Tevatron collider may be written as

$$L = \frac{3\gamma_r f_0}{\beta^*} (BN_p) \left( \frac{N_p}{\varepsilon_p} \right) \frac{F(\beta^*, \theta_x, \theta_y, \varepsilon_p, \varepsilon_{\bar{p}}, \sigma_z)}{(1 + \varepsilon_{\bar{p}}/\varepsilon_p)} \quad (3.6.1)$$

where  $\gamma_r = E/mc^2$  is the relativistic energy factor,  $f_0$  is the revolution frequency, and  $\beta^*$  is the  $\beta$  function at  $s=0$  (where it is assumed to attain the same minimum in each plane). The proton (antiproton) beam transverse emittance  $\varepsilon_p$  ( $\varepsilon_{\bar{p}}$ ) is defined to be  $\varepsilon = 6\pi\gamma_r\sigma^2/\beta$  for a bunch with a gaussian distribution and assumed to be the same in both transverse planes,  $B$  is the number of bunches,  $N_p$  ( $N_{\bar{p}}$ ) is the number of protons (antiprotons) per bunch,  $\theta_x$  and  $\theta_y$  are the crossing half-angles,  $\sigma_z$  is obtained from the rms proton and antiproton bunch lengths  $\sigma_z^2 = (\sigma_{zp}^2 + \sigma_{z\bar{p}}^2)/2$  and  $F \leq 1$  is a form-factor that accounts for the depth of focus (hourglass) and crossing angle effects on the luminosity caused by non-zero bunch lengths. The bunch lengths depend on the longitudinal emittance and the RF voltage, but the luminosity depends only on the bunch lengths. In Run IIa, the form-factor is dominated by the hourglass effect (the design crossing-angle is 0). For Gaussian beams the hourglass effect may be written as:

$$F = \frac{\sqrt{\pi}\beta}{\sigma_z} e^{\frac{\beta^2}{\sigma_z^2}} \operatorname{erfc} \left[ \frac{\beta}{\sigma_z} \right] \quad (3.6.2)$$

where the complementary error function is related to the error function by  $\text{erfc}(z) = 1 - \text{erf}(z)$ . For Run IIb the crossing angle effect is large and the luminosity comes mainly from the  $z=0$  region where the hourglass effect is small. In this case the form-factor  $F$  may be written as

$$F = \frac{1}{\sqrt{1 + \sigma_z^2 (\theta_x^2 / \sigma_x^2 + \theta_y^2 / \sigma_y^2)}} \quad (3.6.3)$$

where  $\sigma_x^2 = (\sigma_{xp}^2 + \sigma_{x\bar{p}}^2) / 2$  and similarly for  $y$ .

The luminosity formula (1) is written to emphasize the major issues in achieving high luminosity. The first quantity in parentheses is the total number of antiprotons. Under current and probably future operating conditions, the most important factor contributing to the achievable luminosity is the total number of antiprotons in the ring,  $BN_{\bar{p}}$ . The second most important factor is the proton phase space density,  $N_p / \varepsilon_p$ , which is constrained by the need to limit the beam-beam tune shift. The form-factor ( $F$ ) and the emittance ratio factor  $\varepsilon_p / (\varepsilon_p + \varepsilon_{\bar{p}})$  are important, but they cannot exceed unity and the amount of luminosity that can be gained using these factors is limited.

### 3.6.1.1.2 Beam-Beam Effects

The formula for the (linear) antiproton beam-beam tune shift (and equal non-linear tune spread) with no crossing angle is:

$$\Delta\nu = 6 \frac{r_p}{4\pi} n_c \frac{N_p}{\varepsilon_p} = 0.0073 (\pi \text{ mm} \cdot \text{mrad} / 10^{10}) n_c \frac{N_p}{\varepsilon_p} \quad (3.6.4)$$

where  $r_p$  is the classical proton radius ( $1.535 \times 10^{-18}$  m) and  $n_c$  is the number of interaction points. Note that the Tevatron functions with antiproton and proton bunches executing helical orbits such that at all points except the interaction points, the counter rotating bunches are transversely separated. Operating experience in the Tevatron Run I suggests that the maximum tolerable beam-beam tune shift lies in the range 0.020 to 0.025. When the beam-beam tune shift is caused primarily by head-on interactions at zero crossing-angle, the beam-beam tune shift determines the maximum value of the factor  $N_p / \varepsilon_p$ , which appears in Eq (3.6.1)

The biggest change from Run I is the increase from 6 to 36 and later, in Run IIb, to hundreds of bunches per beam<sup>40</sup>. 36 bunches per beam correspond to a minimum bunch spacing of 396 nsec. In Run IIb, the minimum bunch spacing will be 132 ns. The peak luminosity achieved during Run Ib was  $2.8 \times 10^{31} \text{ cm}^{-2} \text{ sec}^{-1}$ . For 6x6 operation, this corresponds to about 4.9 inelastic interactions per bunch crossing. Multiple interactions per crossing (IC) make the triggering, the event reconstruction, and physics analysis more difficult. Generally, CDF and D0 detectors would prefer no more than 5 IC. The limit on the number of ICs, combined with the desire for more luminosity, pushes the collider to more bunches.

The main beam-beam concern for multi-bunch operation is that, because bunches are not evenly spaced around the ring, different bunches within a train encounter the

bunches in the opposing beam at different places around the ring. (Proton and antiproton beams share the same vacuum pipe and, in addition to the two main interaction points at B0 and D0, there are many near misses.) This causes differences between bunches in the train. Because of much higher intensity in the proton beam, the antiprotons suffer most from the beam-beam effects.

Figure 3.6.1 shows the tune spreads for all pbar bunches under Run IIa and IIb conditions<sup>41</sup>. The tuneshifts for pbars with zero betatron amplitudes are shown as open circles. Gaussian distributions for the horizontal and vertical displacements and angles of pbars are assumed. From these we calculated their horizontal and vertical betatron amplitudes, and then interpolated between previously calculated tuneshifts with amplitudes for each pbar. The darker the spot in Figure 3.6.1, the more antiprotons have those tunes. As seen from Figure 3.6.1, the bunch-to-bunch (linear) tune shift and intrabunch (non-linear) tune spread are:

$$\begin{array}{lll} \Delta v_{BB} \approx 0.007 & \Delta v_{NL} \approx 0.025 & \text{for Run IIa} \\ \Delta v_{BB} \approx 0.004 & \Delta v_{NL} \approx 0.008 & \text{for Run IIb} \end{array}$$

During Run IIa, the tune footprints for most bunches are almost identical. However, pbar bunches 1 and 12, 13 and 24, 25 and 36 are shifted from the others because they do not see protons at the first crossing point upstream or downstream of the IPs, respectively. (The filling pattern has 3 fold symmetry, the 2 bunches at a given location in the 3 trains should all behave identically). As a result, the pbars take up more space in the tune plane. This may make it more difficult to find operating conditions that are acceptable for all the pbar bunches. If this becomes an intractable problem, we are considering the possibility of not using (not filling) pbar bunches 1,12,13,24,24, 36. This would give us stores of 36 proton bunches on 30 pbar bunches. There are other problems with this approach, but it is a possibility. An alternative solution is *linear beam-beam compensation* (see below).

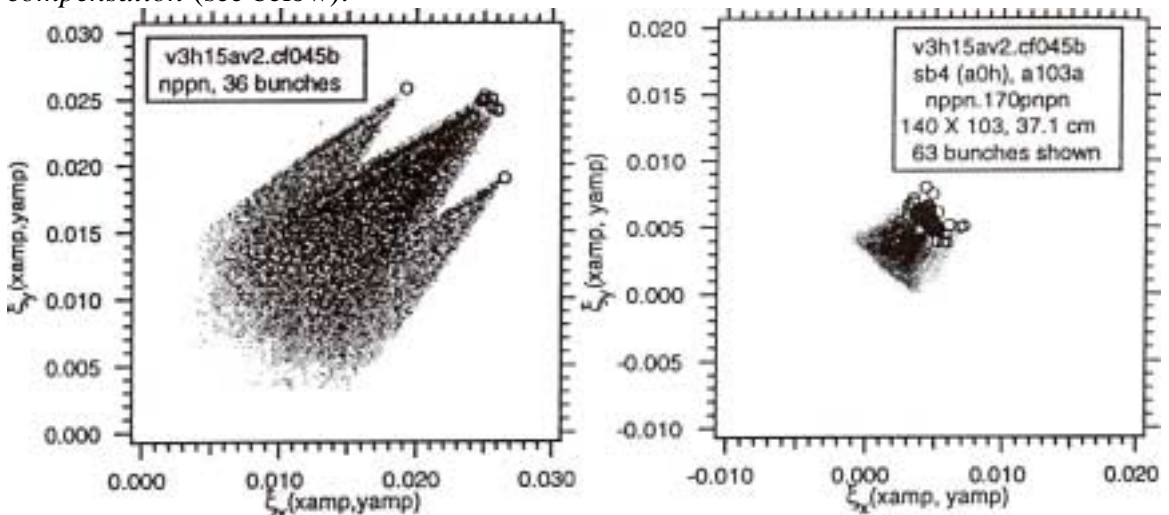


Figure 3.6.1 Gray scale plots showing the tune footprints for all pbar bunches under Run IIa (left) and Run IIb (right) conditions. The darker the point, the more pbars have those tunes. No synchrotron motion for the pbars. The open circles show the tunes for pbars with zero betatron amplitudes.

During Run IIB 140 proton bunches collide with 103 pbar bunches. Because we don't have any symmetry in the 132 ns filling pattern, no two pbar bunches encounter the protons at exactly the same set of crossing points and generally every pbar bunch has a slightly different footprint. The spread between bunches is smaller than for 36x36. That is mainly because the crossing angles have improved the separation at the first few crossing points on either side of the IPs. The footprint in Figure 3.6.1 (right) is "folded". Pbars with horizontal and vertical betatron amplitudes of about  $(4\sigma_x, 4\sigma_y)$  have about the same tunes as those with betatron amplitudes  $(0,0)$ . For small amplitude particles, the tunes decrease with increasing amplitude due to the main IPs and the tune changes due to the first few near misses are small. For larger amplitude particles, the tunes increase with increasing amplitude due to the first few near misses and the tune changes due to the main IPs are small. Taken together, the competition between these effects leads to the fold in the footprint. On the good side, these folds mean that the beam occupies less area in the tune plane and if the resonances have not become stronger and wider, one may have more room in the tune plane between resonances. On the bad side, the folds mean that a particle can have a larger amplitude range for a given range of its tunes. Certain amplitude particles will not detune off the resonances as quickly and so a resonance that aligns with the fold will cause a greater amplitude change than it could without the fold. In summary, the folds are bad signs and indicators of strong nonlinearities.

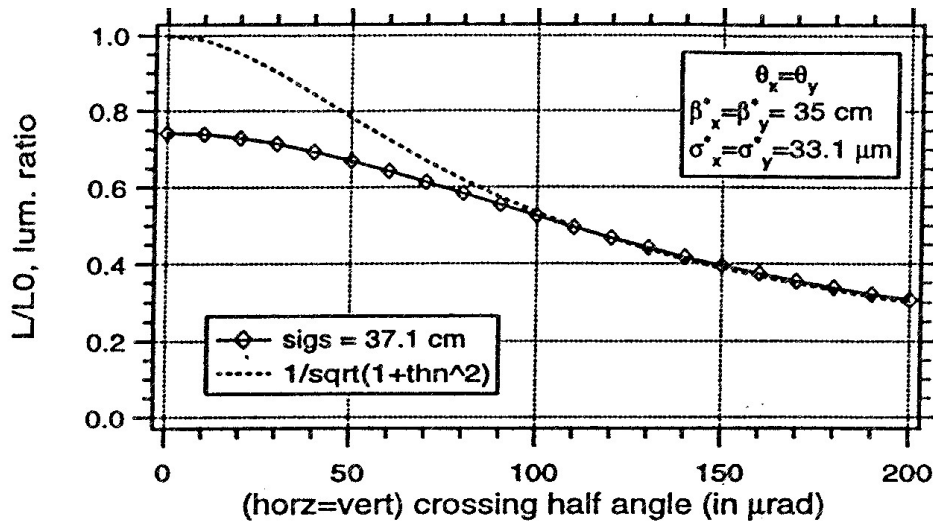


Figure 3.6.2 The luminosity form-factor as a function of angle. The angle is the half-angle in either plane: it is assumed to be the same horizontally and vertically.

For Run IIB, the tuneshift formula Eq. ( 3.6.4 ) does not apply. The beams cross at an angle to avoid unwanted beam-beam interactions near the interaction region. At a bunch spacing of 132 ns, the first crossing points on either side of the main Interaction Points are before the electrostatic separators. The second crossing points are just beyond the separators, but without a crossing angle, the separation at these points is only about  $0.7\sigma$ . Without a crossing angle, for each IP, we would have 3 head on collisions and two crossings with separation of about  $0.7\sigma$ . This is unacceptable and so for this bunch spacing, we require a crossing angle. Because the bunches are very long ( $\sim 37$  cm with the present Tevatron rf system) with very small transverse beam sizes at the interaction point

(about 30. microns), the crossing angles we are contemplating are not small. They have significant effects on the overlap of the beams and hence on the luminosity and beam-beam tune shifts. Figure 3.6.2 shows the form-factor in the luminosity equation as a function of crossing angle.

The dramatic loss in peak luminosity is a strong incentive to keep the crossing angles as small as possible. However, the crossing angle essentially determines the separation at the first 2 crossing points on either side of the IPs (this is the total of 8 crossing points). With both these considerations in mind, we presently plan for half crossing angles of  $\pm 136 \mu\text{rad}$ . in both the horizontal and the vertical plane. This gives a total angle between the beams of  $2^{3/2} \times 136 \mu\text{rad} = 385 \mu\text{rad}$  and corresponds to about  $4\sigma$  at the first crossing points.

There are several implications of these large crossing angles: a) loss of peak luminosity; b) integrated luminosity concerns; c) change in size and shape of the tune footprints from the main IP; d) synchro-betatron resonances driven by the beam; e) strong effects from the first few crossing points as the tune spreads from these points are not small, moreover, since the beams are separated, the beam-beam interaction can drive both even and odd resonances; f) large displacements in low-beta quads which may reduce dynamic aperture.

Besides the footprints, beam-beam dipole kicks are of concern. Each time a bunch encounters a bunch from opposing beam, they both receive kicks. If the beams are separated, then the average kick received by the bunch will be non-zero. The average kicks received by both beams will change their orbits and hence their separation. The change in separation in turn changes the average kicks, which bunches give each other. For 36x36, the separations at the IPs are about  $1.5 \mu\text{m}$  (the beam size at the IPs is  $33 \mu\text{m}$ ), and the total crossing angles are less than  $11 \mu\text{rad}$  (with rms angle spread at the IPs of  $100 \mu\text{rad}$ ). For 140x103, these beam beam dipole kicks result in  $7 \mu\text{m}$  maximum separation at the IP, and the rms separation  $1.6 \mu\text{m}$ .

### **3.6.1.1.3 Integrated Luminosity**

Figure 3.6.2 shows that we expect to lose about a factor of 2 in peak luminosity with  $136 \mu\text{rad}$  crossing angle. But this does not directly translate into a loss of integrated luminosity. Estimates of the sustainable luminosity depend on many factors related to how well the entire accelerator complex is working. The most important factors affecting the performance are the pbar stacking rate and the pbar recycling efficiency. There are a number of strategies, which have been proposed to reduce the instantaneous luminosity while mitigating the corresponding reduction in integrated luminosity. This has is advantageous both for the experiments and for the luminosity lifetime, which aids the mitigation strategies. We do not explore fully the several luminosity leveling schemes but use the following as an example. Figure 3.6.3 shows the dependence of the weekly integrated luminosity on pbar stacking rate into the Accumulator for different Run II operation regimes<sup>42</sup>: 36x36 with the Accumulator only (without pbar stacking in the Recycle Ring); 36x36 with Recycler used for stacking but without pbar recycling; 36x36 with intensity dependent recycling efficiency between 60% and 80% and luminosity leveling to keep the number of ICs at 5; 140x103 with crossing angle; 140x103 without crossing angle.

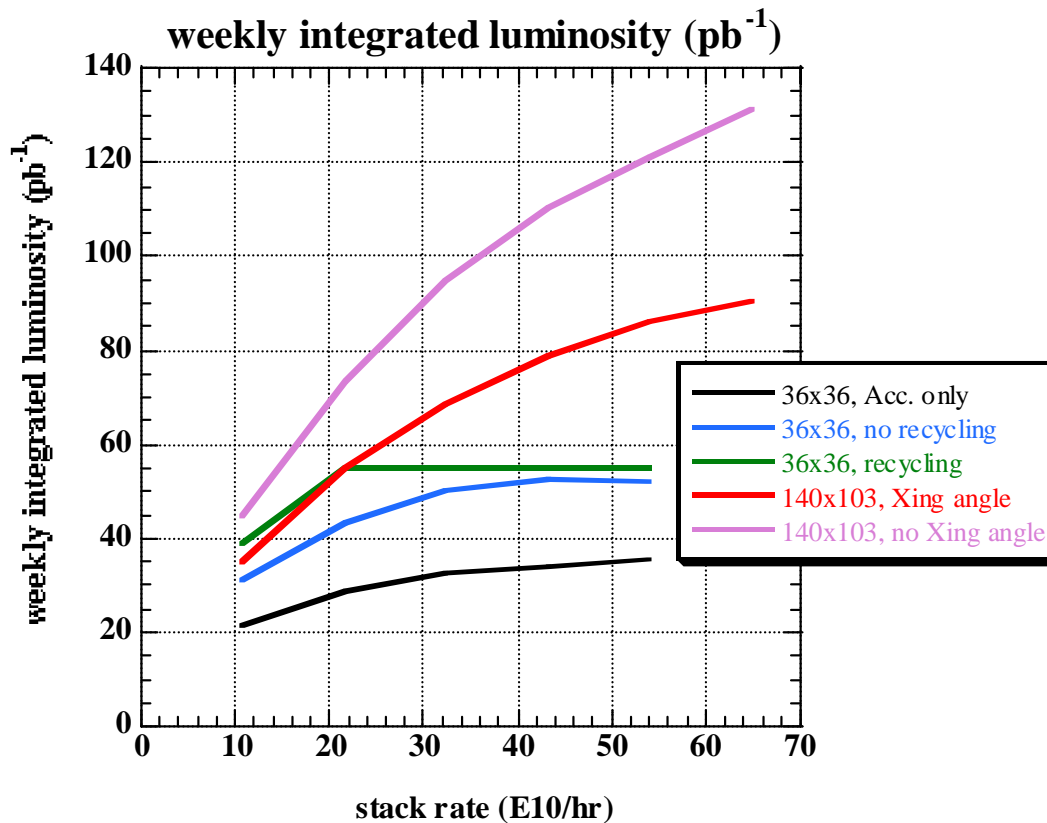


Figure 3.6.3 Tevatron weekly integrated luminosity vs  $p\bar{p}$  stacking rate into the Accumulator. The following assumptions have gone into this plot:

- Accumulator maximum stack size is  $250 \times 10^{10}$ , the stack rate is intensity dependent.
- No Recycler maximum stack size; stack rate is not intensity dependent.
- 8% loss in Accumulator to Recycler transfers.
- Intensity dependent Recycler to Tevatron transfer efficiencies.
- Run II emittances and proton intensities; intrabeam scattering only for growth rates.
- Luminosity counted only within  $\pm 35\text{cm}$  from IR, matching to the silicon detector acceptances
- 70 mb cross section for luminosity
- 3ev-sec,  $20\pi\text{-mm-mrad}$   $p\bar{p}$ s are recycled
- IR crossing angle is  $\pm 136\mu\text{rad}$
- Luminosity levelled to  $\leq 5$  interactions/crossing (@48mb cross section)
- 20% weekly downtime; 1 hour shot-setup time

We conclude that the effect of the crossing angle on the integrated luminosity might be mitigated such that the loss is approximately 30%. While reduced, this is nevertheless substantial. If the Tevatron Lens could reduce this by permitting the use of a smaller crossing angle, the margin would be very welcome.

### 3.6.1.2 Compensation of Beam-Beam Effects with Electron Beams

We have seen above how the beam-beam interaction in the Tevatron collider sets limits on bunch intensity and luminosity. It has been proposed to compensate these effects with use of a counter-traveling low-energy high current electron beams.<sup>43</sup>

Two electron beam setups for compensation of the beam-beam effects in the Tevatron (TEL- Tevatron Electron Lens) are planned to be installed away from the interaction points at B0 and D0. They provide the electron beams which collide with the antiproton beam. The electron beam is created on an electron gun cathode, transported through the interaction region in a strong solenoidal magnetic field, and absorbed in the collector. Since the electron charge is opposite to the proton charge, the electromagnetic force on antiprotons, due to the proton beam, can be compensated by the electron beam. The proton beam has to be separated from the electron and antiproton beams in the device.

There are two implementations of the proposal:

- 1) an “electron lens” with modulated current to provide different linear defocusing forces for different antiproton bunches in order to equalize their betatron frequencies (further referred as *linear compensation*)
- 2) an “electron compressor”, that is a nonlinear DC electron lens which compensates (on average) the nonlinear focusing due to the proton beam – *nonlinear compensation*. The latter has a potential for *crossing angle elimination*.

Initial estimates of the maximum increase in the collider luminosity due to the BBC are based on a simplistic relation between the peak luminosity, the maximum tune area available for operation  $\Delta v_{\max}$ , and the tune spreads, both bunch-to-bunch and intrabunch. That is to say, we can write  $L/L_0 \approx \Delta v_{\max} / (\Delta v_{\text{BB}} + \Delta v_{\text{NL}})$ . In addition we take the maximum footprints permitted, without tune compensation, to be those indicated in Fig. Figure 3.6.1. Assuming that a fully working beam beam compensation scheme can eliminate the bunch to bunch (linear) variation and that the tune spread within each bunch can be reduced by a factor of 2, we can deduce that:

- the *linear* BBC may potentially lead to some 16%-30% increase in peak luminosity with 36x36 bunches in Run IIa and some 50% in Run IIb
- in addition to that, the *nonlinear* BBC has a potential of a 60-100% increase of peak luminosity in Run IIa and Run IIb,
- if the nonlinear BBC will make it possible to eliminate the *crossing angle* by compensating 2 or 4 additional collision points around each IP, that would allow a 2-fold increase in the peak luminosity in Run IIb.

The potential increase in the integrated luminosity is more modest:

- the *linear* BBC may potentially lead to some 8% increase in integrated luminosity in Run IIa with pbar stack rate 40e10/hr and some 12% with 20e10/hr (see Figure 3.6.3) and some 30% in Run IIb
- in addition to that, the *nonlinear* BBC has a potential of a 40% increase of peak luminosity in Run IIa and Run IIb,

- if the nonlinear BBC will make it possible to eliminate the *crossing angle* by compensating 2 or 4 additional collision points around each IP, that would allow to increase peak luminosity by 41% in Run IIb.

It is assumed that  $\Delta v_{\max}$  remains the same and that the required increase, up to a factor 2, in the proton beam intensity is possible. We do not have an idea yet how the BBC will affect the maximum allowable tune area for operation. But the higher proton beam intensity in the Tevatron is definitely of concern.

### 3.6.1.3 Concerns of Higher Proton Intensities in the Tevatron

With this increase in current in the Tevatron, one of the things, which we will have to do, is to maintain the longitudinal stability of the bunches. Even now, at the start of Run IIa, we have already observed bunch oscillations, which persist for a very long time. Although we have not observed that these oscillations grow in time, they do dilute our longitudinal emittance unnecessarily. Therefore, it is important that we solve this problem in Run IIa before proceeding with any upgrade plans with the Beam-Beam Compensation or /and for Run IIb.

Another concern is antiproton lifetime at injection. At present, the Tevatron is having greater difficulties due to reduced antiproton lifetime at 150 GeV. The proton intensity is currently only half of the design value. This may be due to the fact that we have very large antiproton emittances (especially longitudinal) at 150 GeV. In Run I, the 150 GeV antiproton lifetime was also a problem at high proton intensities.

## 3.6.2 Machine Physics

Since 2000, significant progress has been made in analytical studies and computer simulation of the beam-beam compensation in the Tevatron and in experimental studies of impact of the 1<sup>st</sup> Tevatron Electron Lens (TEL) on the 980 GeV proton beam.

### 3.6.2.1 Analytical studies and numerical tracking simulations of the Beam-Beam Compensation with electron beams in the Tevatron collider

Due to a number of reasons, a larger number of protons per bunch, a smaller proton emittance, a factor of seven larger number of the parasitic long-range interactions (see Table 3.6.1), the beam-beam driven resonances (the synchro-betatron ones in particular) can present, in the Tevatron Run IIa configuration, a greater risk of instability of antiprotons than previously.

Another complication associated with the parasitic interactions is the so-called PACMAN effect: dependence of the tunes on the bunch position in a train as illustrated by Figure 3.6.4a which shows the distribution of antiprotons in the tune diagram with the standard Tevatron choice of bare lattice tunes,  $\nu_{x0} = 20.585$ ,  $\nu_{y0} = 20.575$ . Each of the 12 bunches in a train is represented by 3000 particles, tunes were calculated analytically following Ref.[43].

	Run Ib	Run IIa	Run IIb
$N_p$ /bunch, $10^{11}$	2.32	2.7	2.7
$\epsilon_p$ (95% norm.), $\pi \cdot \mu\text{m}\cdot\text{rad}$	23	20	20
$\xi$ /nominal IP	0.0074	0.01	0.01
$N$ parasitic Ips	10	70	278
$\xi$ , total	$\sim 0.015$	$\sim 0.025$	$\sim 0.025$
$\epsilon_{p\text{bar}}$ (95% norm), $\pi \cdot \mu\text{m}\cdot\text{rad}$	13	15	15

Table 3.6.1

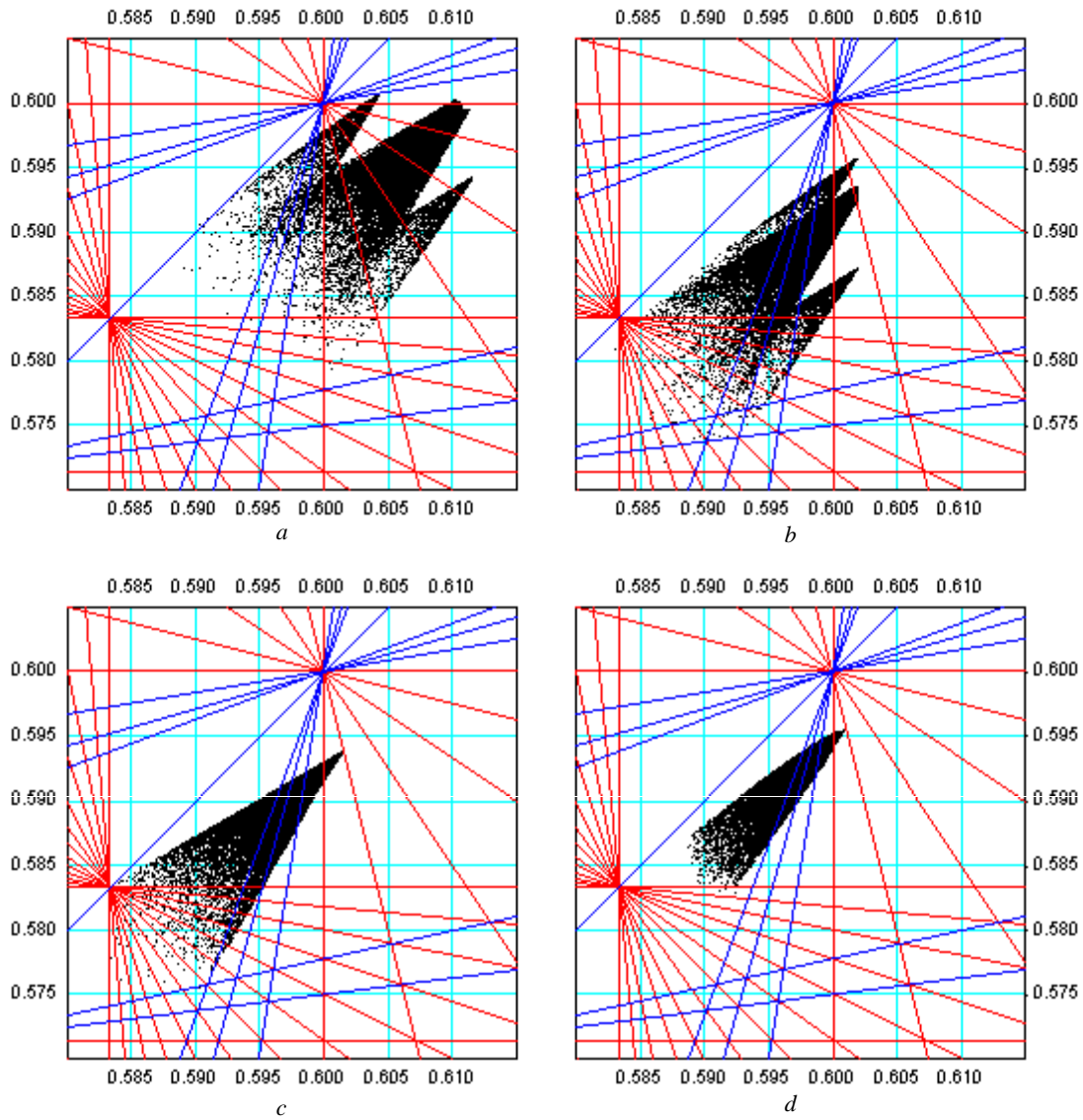


Figure 3.6.4 a) Antiproton beam footprint in the betatron tunes plane with: a – no BBC, b – linear BBC with 1 Tevatron electron lens (TEL), c – linear BBC with 2 TELs, d – nonlinear BBC with 2 TELs

As can be seen from Figure 3.6.4a it is impossible to accommodate all particles in the area free of the resonances of order lower than 13, which are shown as red and blue lines, for the sum and difference resonances respectively.

The beam-beam tuneshift can be compensated with the help of electron lenses [43]. Two linear lenses created by electron beams of constant charge density can completely eliminate the bunch-to-bunch tunespread (linear beam-beam compensation), by choosing a bell-like shape it is possible to reduce the intrabunch nonlinear tunespread as well (nonlinear compensation). However, the question remains as to whether this will really improve the stability of antiprotons, since the electron beams themselves may contribute to excitation of high order resonances remaining within the residual tunespread.

### 3.6.2.1.1 Linear Beam-Beam Compensation

Round electron beam of *constant* charge density acts as a *linear lens* on the antiprotons with amplitudes smaller than its radius  $a_e$  producing negative tuneshift in both transverse planes in proportion to the corresponding betatron function:

$$\Delta\nu_{x,y} = -\frac{1+\beta_e}{\beta_e} \cdot \frac{I_e L_e r_p}{2\pi\gamma_{\bar{p}} e c a_e^2} \beta_{x,y} \quad (3.6.5)$$

, where  $I_e$ ,  $L_e$ ,  $a_e$  and  $\beta_e = v_e/c$  are respectively the electron beam current, length, radius and relativistic velocity.

Current modulation in the electron lens (TEL1) placed at a location where  $\beta_x \gg \beta_y$  allows us to equalize the horizontal tuneshift in all bunches without affecting vertical tunespread. Circles with violet fill in Figure 3.6.5 show what electron current should be applied to each of 12 antiproton bunches under Run IIa conditions in order to equalize the horizontal tuneshifts for small amplitude particles in the case of electron beam with  $a_e = 1.8$  mm,  $\beta_e = 0.2$ ,  $L_e = 2$  m at location where  $\beta_x = 98.7$  m,  $\beta_y = 28.4$  m. The resultant tune distribution is shown in Figure 3.6.4b.

Adding the second electron lens (TEL2) at a location where  $\beta_x \ll \beta_y$  permits us to equalize both horizontal and vertical tuneshifts. The electron currents which are needed in this case are shown in Figure 3.6.5 by circles with blue and red fill. The radius of the second beam is  $a_e = 2.35$  mm, at its location  $\beta_x = 56.7$  m,  $\beta_y = 172$  m. The resultant tunespread is shown in Figure 3.6.4c.

Though the electron beam radii were chosen sufficiently large (more than  $3\sigma_{pbar}$ ) the stability of particles in the tails of the beams, which see the sharp edges of the electron beams, is not guaranteed. The effect of the electron beam size and profile was a subject of extensive numerical simulations with the LIFETRAC code<sup>44</sup>. One example of simulation results is presented in Figure 3.6.6, where the contour plots of p-bar distributions in  $A_x$ ,  $A_y$  plane are shown. The distance between successive contour lines is  $\sqrt{e}$ . Each step corresponds to 300,000 turns (6 seconds of real time in the Tevatron), 3000 particles were tracked. The data gathered are averaged over all the particles, all the turns, approximately one billion particle-turns for each step. The last column presents the effect of the TEL, which is applied at “bad” working point (0.566,0.556) and shifts tunes by 0.01 toward a “good” one. One can see the positive effect of the application of the lens in the differences between the pbar distributions at the corresponding working points

without e-lens, in columns marked as “bad” and “good”, and those with the lens operational, marked as “bad” +TEL. Several electron current density profiles considered including Gaussian and those described by the formula:

$$\rho(r) = \rho_0 \frac{1 + \alpha(r/R_0)^2}{1 + (r/R_0)^n} \quad (3.6.6)$$

with  $\rho_0$  adjusted so as to keep  $\Delta v_{x,y} = -0.01$  at different values of parameters  $\alpha$  and  $n$ . The bare lattice tunes, after some scanning, were chosen to be  $\nu_{x0} = 20.566$ ,  $\nu_{y0} = 20.556$ . Tracking with noise showed high sensitivity to and complicated dependence on the electron beam profile. A number of other issues were addressed in the simulations with one TEL: effect of the e-beam misalignment (meanders and offsets) and noise as well as the transient effect while aligning the e-beam with the orbit of antiprotons.

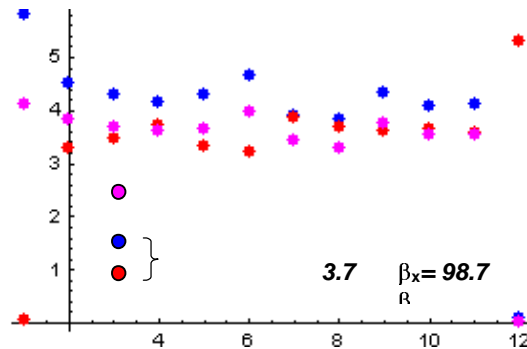


Figure 3.6.5 *Electron beam currents needed for equalization of the horizontal tunes with one TEL (violet) and both horizontal and vertical tunes with two TELs (blue and red).*

The results can be briefly summarized as follows:

- a) electron beam size has to be at least about 3 times the rms antiproton beam size  $R_0 \approx 3\sigma_{pbar}$  for good beam lifetime and small emittance growth
- b) Stationary offsets of up to  $0.2 R_0$  are tolerable
- c) meandering of the electron beam around the  $\bar{p}$  orbit with amplitude of  $0.25 R_0$  produces no harmful effect; this opens a possibility to vary the e-beam effective aspect ratio by deliberately bending the beam with correctors
- d) the process of the electron beam alignment, if started from large initial offsets ( $\geq R_0$ ), destroys the antiproton beam, therefore it has to be done in a few steps, each time with a new  $\bar{p}$  bunch and/or using initially lower electron beam current
- e) the  $\bar{p}$ -beam emittance dilution due to random turn-by-turn fluctuations in the e-beam position and current is found to be in a good agreement with the previous analytical estimates<sup>43</sup>, for example, the relative current fluctuation of  $dJ/J = 2.2 \cdot 10^{-3}$  results in 10 hrs emittance growth time due to the noise.

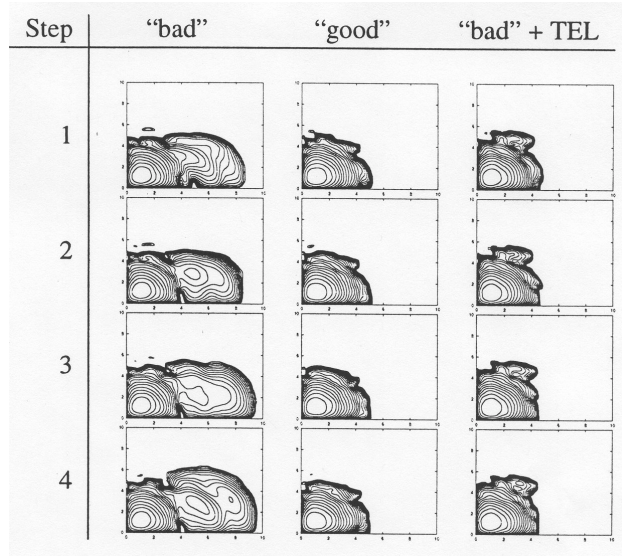


Figure 3.6.6 Distribution of the pbar-beam in the plane of normalized betatron amplitudes after (1,2,3,4) x 300,000 turns.

### 3.6.2.1.2 Compensation of Nonlinear Beam-Beam Effects

Compensation of non-linear beam-beam effects requires shaping the electron beam profile by application of negative voltage to a near-cathode Pierce-like electrode (a “profiler”) or by changing geometry of anode and cathode. The beam produced will have a smaller r.m.s. size and smoother edges as shown in Figure 3.6.7, lines 2,3 and 4. As a result:, the intrabunch nonlinear tunespread is partly compensated and it is less difficult to accommodate the total footprint in a resonance free area. Compared to the linear BBC (see corresponding profile in Figure 3.6.7, line 1), there is weaker excitation of high order resonances for antiprotons with large betatron amplitudes, which see the electron beam edges. The electron beam current required for the smaller beam radius is smaller and electrostatic space charge effects in the electron beam are therefore weaker.

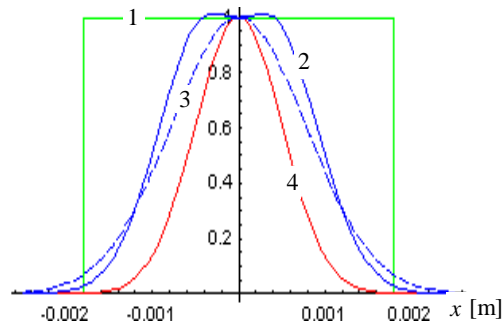


Figure 3.6.7 Space Charge distribution: 1- linear TEL, 2- TEL with “profiler” 3- Gaussian distribution with the same current, 4- antiproton beam at TEL 1

With the electron and antiproton beam sizes becoming comparable, there appears a strong amplitude dependence of the tuneshifts produced by a Tevatron electron lens (TEL) as shown in Figure 3.6.8. It counteracts the tuneshift of particles with significant amplitudes resulting from the head-on collisions with the proton beam thus leading to a compression of the total tunespread within a single antiproton bunch (*the nonlinear beam-beam compensation*).

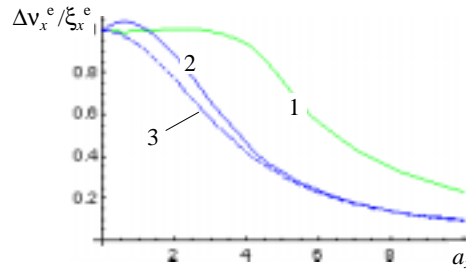


Figure 3.6.8 *Pbar* normalized horizontal tuneshift due to TEL with *e*-beam profiles as shown in Figure 3.6.7.

Obviously, to fully benefit from such compensation, one should eliminate the bunch-to-bunch tunespread first, so two electron lenses would be necessary: TEL1 at location with larger horizontal  $\beta$ -function ( $\beta_x = 98.7\text{m}$ ,  $\beta_y = 28.4\text{m}$ ) and TEL2 at location with larger vertical  $\beta$ -function ( $\beta_x = 56.7\text{m}$ ,  $\beta_y = 172\text{m}$ ). To begin with we have chosen the electron beam sizes (HWHM) to be  $r_e = 1\text{mm}$  in TEL1 and  $r_e = 1.3\text{mm}$  in TEL2. The electron currents, which provide a complete compensation of the bunch-to-bunch tunespread and compress the intra-bunch nonlinear tunespread by a factor of two are shown in Figure 3.6.8. Due to smaller *e*-beam sizes they are twice lower than needed for the linear BBC.

The effect of TELs on the nonlinear tunespread is illustrated by Figure 3.6.10, which shows the antiproton bunch #6 footprint in the tune diagram without BBC (black) and with it (teal blue). The bare lattice tunes (assumed nominally to be  $\nu_x = 20.585$ ,  $\nu_y = 20.575$ ) were slightly trimmed in the latter case. The arc lines correspond to equidistant with step 2 values of the total transverse amplitude

$$a_{\perp} = \sqrt{a_x^2 + a_y^2} \quad (3.6.7)$$

where  $a_{x,y}$  are taken in the *pbar*  $\sigma$ 's, the radial lines correspond to constant values of  $a_x/a_y$ . The red and blue lines show respectively sum and difference resonances of orders lower than 13.

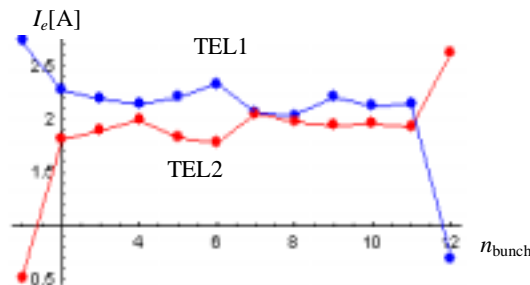


Figure 3.6.9 *Electron currents in the two TELs as seen by different antiprotons*

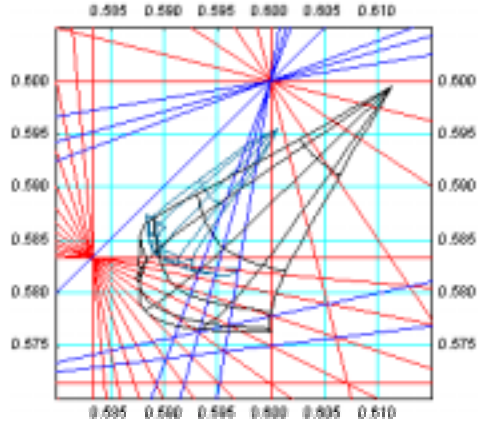


Figure 3.6.10 Original and compressed pbar bunch #6 footprint around nominal working point.

It can be seen that the footprint “folding”, which is caused by the long-range interactions with the proton beam and without BBC happens at amplitudes  $\sim 8\sigma$ , with BBC takes place at amplitudes as low as  $5\sigma$ . Since even very weak high order resonances may lead to a fast particle transport over the region of folding thus reducing the pbars lifetime, this effect sets a natural limit on the degree of the footprint compression. Another limitation comes from the requirement that the tune modulation by the synchrotron motion due to finite dispersion at the TEL locations was small:  $r_e \gg D_x \sigma_E \approx 1.7\text{m} \times 9 \cdot 10^{-5} \approx 0.15\text{mm}$ , to avoid strong excitation of the synchrotron satellites of betatron resonances.

The electron beams of TELs can themselves contribute to excitation of resonances. Figure 3.6.11 shows beatings of the betatron amplitudes (calculated analytically in a single resonance approximation) due to resonances encountered by antiprotons of bunch #6 whose footprint with BBC was shown in Figure 3.6.10 in teal blue.

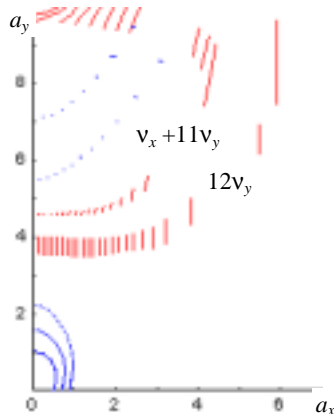


Figure 3.6.11 Swing of the betatron amplitudes due to resonances encountered by pbars of bunch #6 at the nominal working point with BBC.

Due to the TEL contribution the width of the  $12\nu_y$  resonance is much larger than that of the  $\nu_x+11\nu_y$  resonance which, in the absence of misalignments, is excited exclusively by the long-range interactions. For off-momentum particles the effective resonance width is even larger owing to the synchrotron satellites.

#### Choice of the working point

The footprint, when compressed by the TELs, can fit into other areas in the tune diagram which are surrounded by less dangerous resonances. One such possibility, with the tunes around  $\nu_x=20.563$ ,  $\nu_y=20.557$ , was considered for the linear BBC. However, this area is not wide enough to avoid setting some particles on either 7<sup>th</sup> or 9<sup>th</sup> order resonances. Another option is the SPS working point  $\nu_x=20.689$ ,  $\nu_y=20.682$ .

#### Effect of the electron beam profile

Excitation of the 16<sup>th</sup> order resonances (and its satellites) by TELs can facilitate diffusion of antiprotons, especially in the region of amplitudes where the footprint folding occurs. As the example of  $10\nu_x+6\nu_y$  resonance shows, excitation of high order resonances by TELs can be reduced by making the e-beam charge distribution more monotonous (e.g. Gaussian). One more advantage is that the footprint folding occurs at somewhat larger amplitudes with the Gaussian e-beams. Analytical calculation of the beatings of the betatron amplitudes at the SPS working point in the case of Gaussian e-beams predicts only moderate effect of the difference resonance  $3\nu_x-6\nu_y$  on the tail particles.

#### Effect of the number of TELs

There is an additional argument (besides compensation of the PACMAN effect) in favor of using two TELs at points with  $\beta_x \gg \beta_y$  and  $\beta_x \ll \beta_y$  rather than one TEL at a location with equal  $\beta$ s. From the resonances excited by TELs the high-order sum resonances are the most dangerous (the WP can always be chosen so that the uni-dimensional ones were reached at too small amplitudes to be noticeable or not reached at all). Since the driving term of the  $k\nu_x+l\nu_y = n$  resonance contains the factor  $\beta_x^{k/2}\beta_y^{l/2}$ , its excitation is significantly suppressed in the case of two TELs. In all cases TELs provided the same horizontal tuneshift  $\Delta\nu_x = -0.014$ .

#### Effect of the finite dispersion

Owing to the finite dispersion TELs can contribute to excitation of the synchro-betatron resonances (SBRs) in two ways: via the tune modulation arising from the steep fall-off of the instantaneous tuneshift with the displacement  $D_x\delta_p$ , and via variation of the nonlinear component of the TEL field seen by an antiproton in the course of the synchrotron motion. According to the estimates the second effect should not be important, whereas the first one, the TEL second order chromaticity, is big: TEL tuneshift is modulated by more than 20% at  $a_s = 3$ . Both effects can be reduced, if necessary, by increasing the e-beam radius.

#### Numerical simulations

All the above presented results were obtained in the single resonance approximation using analytical formulae<sup>45</sup>. More realistic picture can be obtained by tracking simulations with the code LIFETRAC which can take into account the cooperative action all beam-beam and TEL nonlinearities and the external noise.

Figure 3.6.12 shows the evolution of the density of bunch #6 at the SPS working point with the BBC by two Gaussian TELs which provide zero-amplitude tuneshifts of  $\Delta\nu_x^e \approx -0.0144$ ,  $\Delta\nu_y^e \approx -0.0115$ . With the bare lattice tunes 20.689, 20.682 the 13<sup>th</sup> order resonances proved to be strong enough to affect the core particles (left column). With tunes shifted down by 0.005 (center column) the core was not affected, still some tails had developed which were not seen in the test run with linear lenses instead of TELs. Weakening the TELs nonlinearity by a 15% increase in the e-beam sizes diminishes the tails (right column). In none of these cases had luminosity or lifetime suffered.

### Conclusions

- With the help of two electron lenses it is possible to completely compensate the bunch-to-bunch tunespread (PACMAN effect) and partially reduce the intrabunch nonlinear tunespread.
- The degree of nonlinear BBC is limited by the footprint “folding” due to the long-range contribution and the electron lens chromaticity due to finite dispersion.
- The possibility to eliminate the folding of the footprint by additional compensation of the long-range interactions (e.g. with pulsed wires) should be studied.
- Excitation of high order resonances by TELs can be reduced by choosing a smooth electron beam charge distribution (e.g. Gaussian) and using two TELs at points with strongly unbalanced  $\beta$ -functions.
- Compression of the footprint by a factor of two permits it to fit in areas free of resonances of order less than 13; the neighborhood of the SPS working point is a promising candidate.

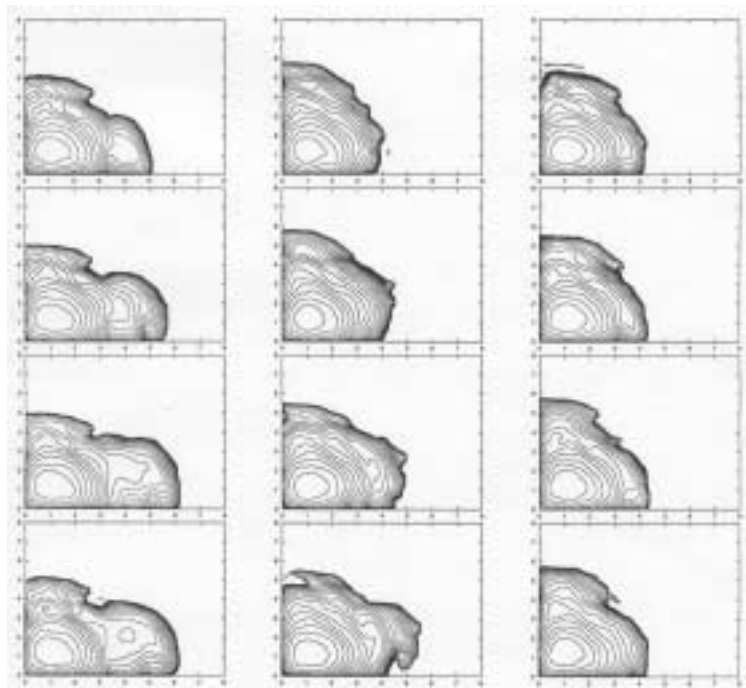


Figure 3.6.12 *Evolution of the pbar density under impact of TELs.*

### 3.6.2.2 Tevatron Electron Lens Studies with 980 GeV protons

In 2001 the first Tevatron electron lens (TEL) has been installed in the Tevatron, commissioned, and demonstrated the theoretically predicted shift of betatron frequencies of a high energy proton beam due to a high current low energy electron beam. After the first series of studies in March-October 2001, we achieved tuneshifts of 980 GeV protons of about  $dQ=+0.007$  with some 3 A of the electron beam current while the proton lifetime was in the range of 10 hours (some 24 hours at the best). Future work will include diagnostics improvement, beam studies with antiprotons, and fabrication of the 2nd TEL.

#### 3.6.2.2.1 Description of the TEL-1

Figure 3.6.13 depicts a general layout of the TEL. The magnetic system of the TEL (see details below in Section 3.6III.A) consists of a 65 kG SC main solenoid, four 8 kG and two 2 kG SC dipole correctors in the same cryostat, and 4 kG gun and collector solenoids. The TEL cryostat is part of the Tevatron magnet string cooling system. A strong  $\Pi$ -shaped magnetic field is needed to guide 10 kV electron beam from an electron gun thru an interaction region, where electrons collide with high energy (anti)protons, to a water cooled collector. SC dipole correctors allow precise steering in position and angle of the electron beam onto the Tevatron beams. A number of precautions have been taken during SC magnets fabrication in order to achieve very high linearity of magnetic field lines inside the main solenoid. The reason is that as the electron beam goes along magnetic field lines it should not deviate around the straight Tevatron beam trajectory, otherwise the effectiveness of the TEL would be deteriorated.

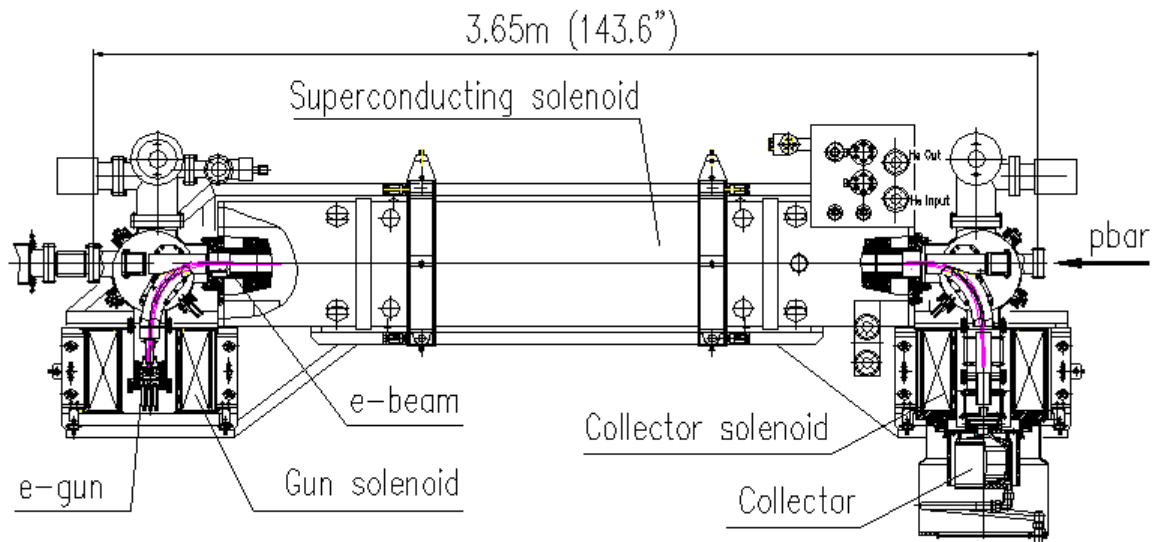


Figure 3.6.13 General layout of the Tevatron Electron Lens.

Measured rms deviations of the lines are  $15\ \mu\text{m}$  in the vertical plane and  $50\ \mu\text{m}$  in the horizontal plane (which is the plane of the bends). This is 10% of the Tevatron beam size in the location of the electron lens. It was found experimentally that the electron beam can be steered to pass through the main solenoid if the gun solenoid field is in the range of  $B_{Gun}=1.9\text{-}4.2\ \text{kG}$  for  $B_m=35\text{kG}$  (outside the range, the beam touches parts of the vacuum system).



electrodes) and discontinuities of the beam pipe all together generate a broadband impedance  $|Z/n| < 0.1$  Ohm, that is a very small contribution to the total Tevatron impedance estimated to be some 2-8 Ohm.

In March-October 2001 there was a total of twelve 8-hour beam shifts dedicated to studies with the Tevatron Electron Lens. Most experimental results were obtained with a single coalesced proton bunch in the ring at the energy of 980 GeV. In the text below, 980 GeV should be assumed unless otherwise stated. The total proton bunch length was less than 19 ns; the bunch intensity varied from 6 to  $60 \times 10^9$ . The only shift at 150 GeV on March 23 was the very first one and to our great satisfaction a decent betatron frequency shift was observed, breaking the path for application of electron lenses in high-energy accelerators.

### 3.6.2.2 Proton Tune Shift due to TEL

According to [43], a perfectly steered round electron beam with a constant current density distribution will shift the betatron tune by:

$$dQ_{x,y} = \mp \frac{\beta_{x,y}}{2\pi} \cdot \frac{1 \pm \beta_e}{\beta_e} \cdot \frac{J_e L_e r_p}{e \cdot c \cdot a_e^2 \cdot \gamma_p} \quad (3.6.8)$$

where the sign reflects defocusing for antiprotons and focusing for protons,  $\beta_e = v_e/c$  is the electron beam velocity,  $\beta_x = 101$  m and  $\beta_y = 28$  m are the  $\beta$  functions at the location of the lens (the first TEL is installed in the Tevatron sector F48).  $a_e$ ,  $J_e$  and  $L_e$  stand for the electron beam size, current and effective interaction length,  $r_p$  is the classical proton radius, and  $\gamma_p = 1044$  is the relativistic Lorentz factor for 980 GeV protons. The electron beam is assumed to be much wider than the (anti)proton beam, so that all the high-energy particles acquire the same  $dQ$ . The factor  $1 \pm \beta_e$  reflects the fact that the contribution of the magnetic force is  $\beta_e$  times the electric force contribution and depends on the direction of the electron velocity. So far we operated with protons only (while the actual goal is to operate with antiproton bunches) which move in the same direction as the TEL electrons, so the magnetic force reduces the total tuneshift.

Figure 3.6.14 shows an example of the Schottky spectra of horizontal proton beam oscillations without electron current and with 3 A electron current. One can see that the horizontal tune is shifted positively by about  $dQ_x = +0.0065$  from 20.5824 to 20.5889. One should expect that the same electron beam would shift the horizontal tune of antiprotons  $(1 + \beta_e / 1 - \beta_e) = 1.5$  times this amount, i.e., by -0.01 given that  $\beta_e \approx 0.2$ . Besides a central peak corresponding to the betatron frequency (highlighted by marker line), the spectra consist of several synchro-betatron sidebands, separated by the synchrotron tune  $Q_s \approx 0.0007$ . The total power in the peaks depends on proton intensity and noise level exciting the beam motion. The application of the electron beam may or may not cause the spectrum shape variation seen in Figure 3.6.2. The shape also depends on the machine tuning, working point. The shape variations sometimes make precise tuneshift measurements rather difficult, and we estimate typical error to be  $\delta Q \approx \pm 0.0001$ .

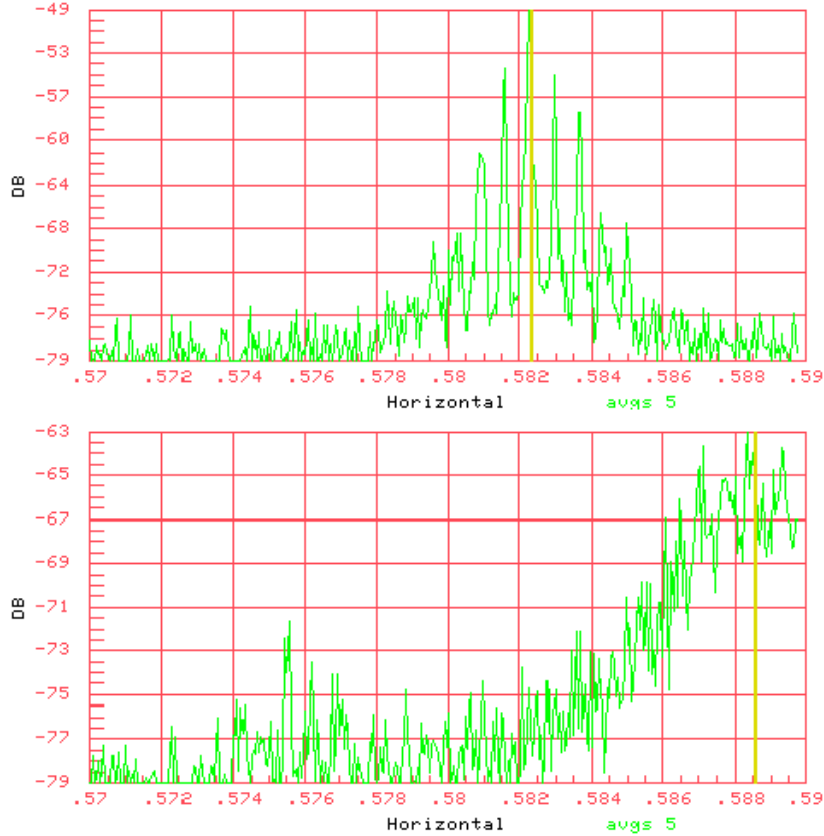


Figure 3.6.14 Schottky spectra of horizontal motion of protons without electron current (top) and with 3A of electron current (bottom), cathode potential  $U_c = 7.6$  kV .

Figure 3.6.15 shows how the proton tune shifts depend on the time delay between the electron pulse and the arrival of the proton bunch. One can see that a) the tune shift follows the electron pulse shape and, therefore, it's possible to shift the tune for any bunch without touching neighbors 396 ns distant, and b) the horizontal tune shift is some 4 times the vertical one.  $dQ_x/dQ_y = 0.0037/0.0008 = 4.6$ , close to the  $\beta$  function ratio  $\beta_x/\beta_y=101/28=3.6$ . The remaining difference can be explained by either uncertainty in  $\beta$  functions, which is known to be  $\pm 10\%$  , a small ellipticity of the electron beam, or mis-steering of the electron beam, which might play role if compared with  $a_e$ .

Having the electron beam properly synchronized for maximum effect, we have studied dependence of  $dQ_x$  on the peak electron current. The results are presented in Figure 3.6.16 and compared with Eq. ( 3.6.8 ). The theoretical dependence is non-linear because the electron energy inside the vacuum pipe and, thus,  $\beta_e$ , goes down with the current due to electron space charge,  $U_e=U_c-gQ_{sc}$ , where  $g$  is the geometry dependent factor. As seen in Figure 3.6.4, the maximum discrepancy is about 20% at  $J_e=2$  A. There are systematic errors in a number of parameters used for calculations, e.g.,  $a_e^2$  is known within  $\pm 10\%$ , effective length  $L_e$  depends on precision of the steering and may vary within  $\pm 10\%$ , and the electron current calibration each contribute some  $\pm 5\%$  error. In addition there might be some  $\pm 5\%$  uncertainty in the electron velocity  $\beta_e$  due to formation of an ion cloud, which shields some fraction of the electron space-charge  $Q_{sc}$ . An indication is that the maximum electron current allowed to propagate through the beam

pipe at a given cathode potential of 7.5 kV goes down by 25% if the pulse repetition rate is reduced from 47.7kHz (standard regime of operation with a single proton bunch) to about 50 Hz. On the other hand, ions do not change *charge density* and thus do not contribute to  $dQ$  directly most probably because of larger transverse size of the cloud.

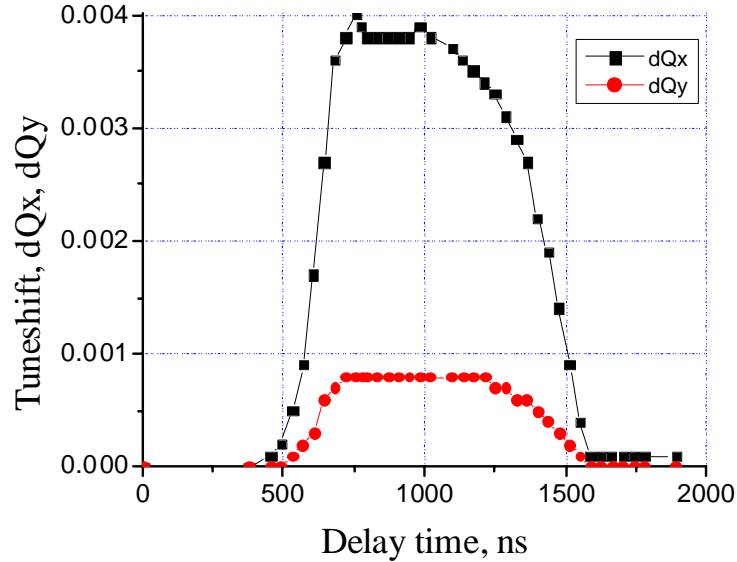


Figure 3.6.15 Shift of the horizontal (black) and vertical proton tunes vs delay between the proton bunch and 800 ns long, 1.96 A peak electron pulse,  $U_c = 6.0$  kV.

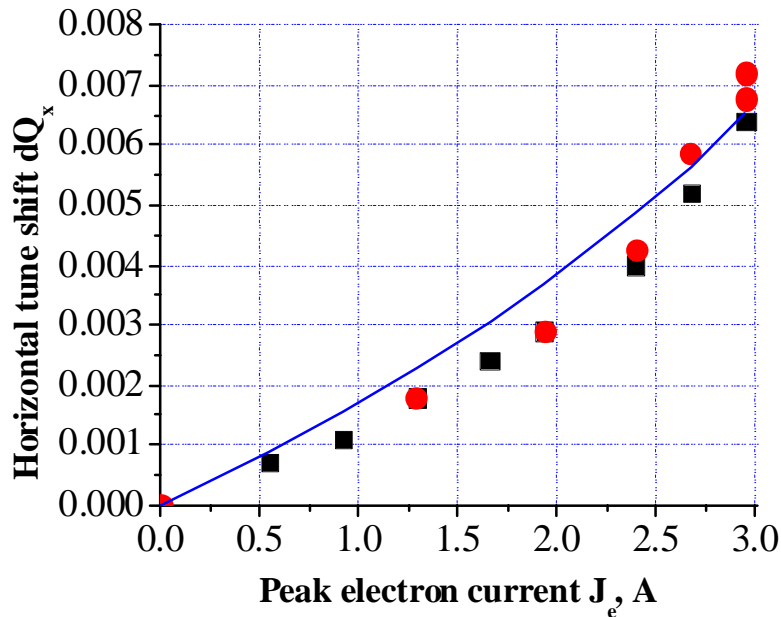


Figure 3.6.16 Shift of the horizontal proton tune vs the electron current,  $U_c = 7.5$  kV. Circles and squares – experimental data, solid line – Eq. ( 3.6.8 )

It might be of interest to mention, that horizontal tune shift for protons coming just after the electron pulse (delay times from 0 to 400 ns in Figure 3.6.15) is slightly lower than  $dQ_x$  for protons arriving right before the electron beam enters the interaction region (delay times above 1600 ns). The little difference of about  $-0.0001$  can be associated with defocusing effect due to ions freshly attracted inside the electron beam.

As long as the proton beam travels inside a wider electron beam, the proton tune shift does not depend much on the electron beam position, e.g., for the case of a 1 A electron beam  $dQ_x(d_x, d_y) \approx dQ_{max} = 0.0021$  if  $|d_{x,y}| < 2\text{mm}$  – see Figure 3.6.17. But when the distance between the centers of the two beams exceeds the electron beam radius then one should expect  $dQ_x(d_x, d_y=0) \approx -dQ_{max}/(d_x/a_e)^2$ ,  $|d_x| > a_e$ , and  $dQ_x(d_x=0, d_y) \approx +dQ_{max}/(d_y/a_e)^2$ ,  $|d_y| > a_e$  (note the sign). Theoretical predictions  $dQ_x(d_x, d_y)$ , see smooth curves in Figure 3.6.17, are in a good agreement with experimental data. The only visible discrepancy is an asymmetry in  $dQ_x(d_x, d_y=0)$ . At negative horizontal displacements,  $d_{x,y} < -2.5\text{mm}$ , the tuneshift does not change sign as it does at  $d_{x,y} > +2.5\text{mm}$ . The effect is, most probably, due to the asymmetric  $\Pi$ -shape of the electron beam trajectory (see Figure 3.6.13), which results in additional positive contribution to  $dQ_x$  from the bending portions of the beam if the protons propagate through them. To summarize, the experimentally observed tuneshifts reasonably well agree with theory.

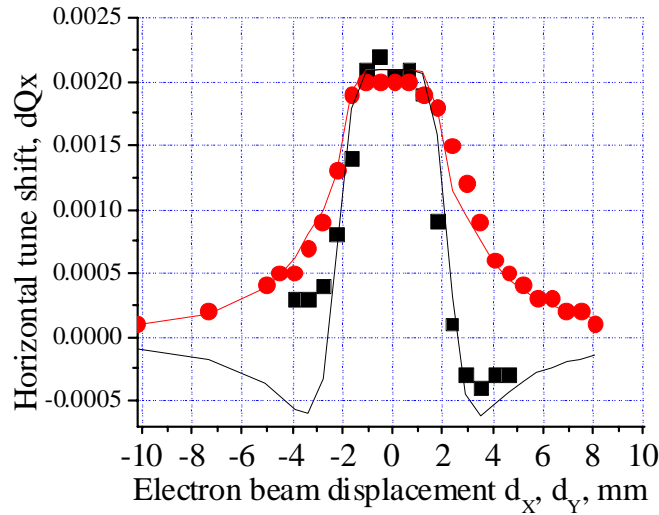


Figure 3.6.17 Horizontal tune shift vs horizontal (squares) and vertical (circles) displacement of the electron beam,  $J_e = 1\text{A}$ ,  $U_c = 6.0\text{ kV}$ .

### 3.6.2.2.3 Proton Lifetime with TEL

There is no formula to estimate the (anti) proton beam lifetime  $\tau = (dN/dt/N)^{-1}$  under impact of the TEL. Nevertheless, analytical studies and numerical tracking predict that the following phenomena affect the lifetime: 1)  $\tau$  depends on non-linear resonances in the vicinity of the machine working point; 2)  $\tau$  should decrease if the electron beam is mis-steered and the protons experience non-linear forces of the electron beam; but if the beam-beam separation is very large, then the electron beam should not affect the lifetime; 3) one should expect better lifetime for the same  $dQ$  if the electron beam is wider and its current density profile is a smooth, bell-like function.

We found that without collisions with the TEL beam, the Tevatron proton beam lifetime is very good over a broad range of the beam parameters and the machine working points (WP)  $Q_x, Q_y$ . Because of the limited time of the studies, we measured lifetimes based on 15 minutes records of the beam intensity. This resulted in some 50% error in  $1/\tau$ , when the typical lifetime was  $\tau_0=90$  hours.

Collisions with the multi-Ampere electron beam always caused some deterioration of the  $\tau$ , but the best lifetime was observed at good WPs. Figure 3.6.18 shows the set of resonances up to 12<sup>th</sup> order over the range  $Q_{x,y}=20.55-20.60$  which is typical for the Tevatron collider operation. The arrows represent the tuneshift due to the TEL. The longest one reflects the result of the very first beam study shift, the very first attempt to operate the TEL with 150 GeV protons. All the others were obtained with 980 GeV protons on different shifts. The numbers near each arrow show the best lifetime achieved at that working point with the maximum electron current. Electron and proton currents and beam sizes were about the same for all these observations, although we can not guarantee that the electron beam was always steered with the same precision.

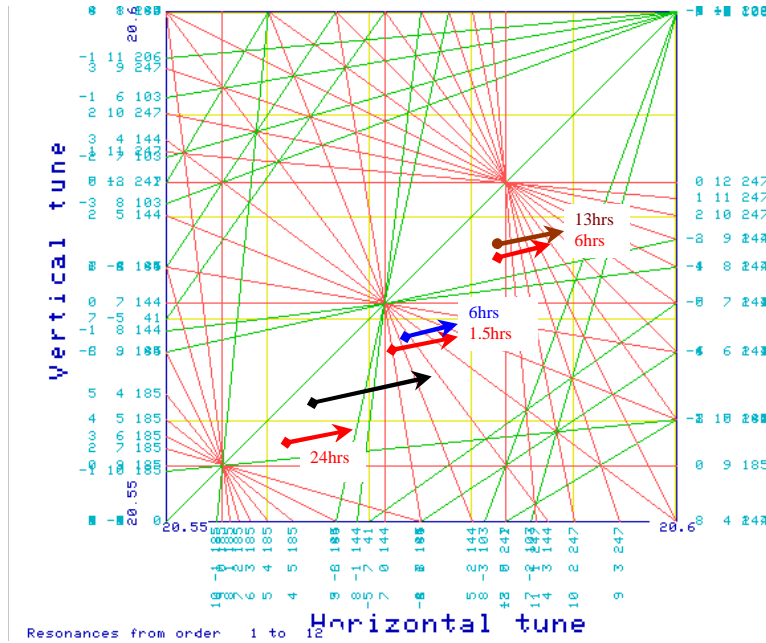


Figure 3.6.18 Proton bunch tuneshifts due to the TEL and corresponding lifetimes.

One can see, that the smallest lifetimes of 1.5-6 hrs were observed when the Tevatron operated at the 7<sup>th</sup> order resonances at  $Q_x, Q_y=0.573, 0.567$ , better lifetimes of 6-13 hours at the 12<sup>th</sup> order resonances  $Q_x, Q_y=0.583, 0.577$ , and the best lifetime of 24 hours was achieved away from resonances at  $Q_x, Q_y=0.564, 0.555$ .

Our experience shows that mis-steering of the electron beam is by far the most important factor affecting the lifetime. It can affect  $\tau$  even at comparatively small electron currents causing the lifetime deterioration when the proton beam crossed the electron beam edges. One may associate these phenomena with the excitation of non-linear resonances. At very large electron currents we also detected significant proton emittance blow-up, which sometime made it impossible to subsequently achieve a good lifetime.

Another factor deteriorating the lifetime is thought to be effective electron current fluctuations, which became quite large when the short pulse FID-pulsar was used. For an electron pulse with about 30 ns rise and fall times and without a clean flat top, 1 ns timing jitter leads to 2-3% variation of the effective electron current fluctuations at betatron frequencies; as shown above, the tolerance is under 0.1%. As a result, the best lifetime observed with the FID pulser was about 4 hours.

On the other hand, if electron and proton beams are separated by some 5 mm (about 3 times the electron beam radius  $a_e$ ), than no deterioration of the proton beam intensity has been observed and the measured lifetime is about  $\tau_0$ .

We did not have enough time to study the effect of the electron beam size and/or electron current density profile yet. The only indication that relative size matters is that when the proton emittance is 1.5-2 times larger than usual, e.g.  $40-60\pi$  mmmrad (95%) instead of  $25\pi$  mmmrad (corresponding to a rms horizontal beam size at the TEL location of 0.8-0.9 mm instead of typically 0.7 mm – compare with  $a_e = 1.75$  mm), the lifetime becomes very poor.

#### ***3.6.2.2.4 Future Studies, Improvements***

Topics for our further studies include: effects of the electron beam size and shape on the tunes and lifetime, emittance growth vs electron beam current and position stabilization, effects of ions, TEL operation with the Tevatron antiproton beam, and, finally, the TEL operation with many bunches. The ultimate goal of the studies is to achieve the same or better pbar lifetime with the TEL at  $dQ$  comparable with the Tevatron beam-beam tune shift and around typical working points.

We also look forward to having more reliable proton diagnostics for the emittance measurements (e.g., synchrotron light system instead of flying wires) and an automated tune measurement system for the multi-bunch measurements. R&D on the better electron beam for the TEL include a wider beam with smooth edges from new 10A, 30kV electron gun pulsed by solid-state HV FID-pulsar, and a better stabilization of the beam current and position.

### **3.6.2.3 Instabilities due to Electron-Antiproton Beam-Beam Interaction**

#### ***3.6.2.3.1 Electron Beam Distortions in Beam-Beam Compensation Set-Up***

Collision with a round antiproton bunch in a strong magnetic field conserves axial symmetry and the radial size of the electron beam. Therefore, the electron beam space charge forces are the same for antiprotons at the head and at the tail of the antiproton bunch. This is no longer true if the electron or antiproton beam is not round. The electron beam axisymmetry can be assured by using a round cathode in the electron gun and by an appropriate choice of the magnetic field in the transport section of the set-up. The antiproton beam roundness could be achieved only in a number of Tevatron locations where vertical and horizontal  $\beta$  functions are the same  $\beta_x = \beta_y$ . The latter condition is not fulfilled for locations of TEL-1 and TEL2.

The electron beam cross section becomes a rotated ellipse as the tail of a non-round antiproton bunch passes it, whereas the head of the bunch sees the original undisturbed

round electron beam. Detailed numerical studies of the effect can be found in Ref.[46]. The electron beam distortions are of concern because:

- 1) the distortion of the space-charge forces which play a role in the beam-beam compensation;
- 2) in addition to the desired defocusing effect, electric fields of the elliptic electron beam produce x-y coupling of vertical and horizontal betatron oscillations in the antiproton beam;
- 3) there appears a “head-tail” interaction in the antiproton bunch via higher order wake fields propagating in the electron beam.

The electron beam density distortion due to that effect is calculated to be about [46]:

$$\frac{\Delta\rho}{\rho} \approx \frac{0.2 \cdot [N_{pbar} / 6e10]}{a_e^2 [mm] \cdot B [kG]} \quad (3.6.9)$$

For example, the distortion is about 1.5% for a 1 mm radius electron beam in a B=40kG solenoid field. This value seems tolerable for operation of the electron lenses for the BBC.

### ***3.6.2.3.2 Head-Tail Effect Due to Electron Beam***

Electron space charge forces cause transverse “head-tail” coupling within the antiproton bunch which may lead to a transverse mode coupling instability (TMCI). A detailed theory, analytical studies and numerical simulations of the effect can be found in Ref.[47]. Here we present estimates of the threshold longitudinal magnetic field necessary to avoid the instability, and the dependence of the threshold on electron and antiproton beam parameters.

Low energy electrons can create significant transverse impedance comparable with the intrinsic impedance of the Tevatron ring, and this can result in a collective instability of the antiproton bunch. The electron beam is to be born on an electron gun cathode, transported through the interaction region, and absorbed in the collector. Therefore, each portion of electrons passes through the antiproton beam only once, and only short distance transverse wake fields are of interest. The phenomenon is as follow: if the centroid of the antiproton bunch head collides off the electron beam center, then the electron-antiproton repulsion causes electron motion. As the result, the electron beam has a displacement when it interacts with the tail of the bunch. Thus, the impact of the electron beam on the following antiprotons depends on the transverse coordinate of the preceding antiprotons. Such a “head-tail” interaction leads to the TMCI.

This effect is similar to the "strong head-tail" interaction via vacuum chamber impedance first observed a long time ago in electron storage rings. The TMCI in the electron rings limits the maximum single bunch current. In our case, the source of the coupling is the electron space charge which is the basic mechanism for the beam-beam compensation and, thus, can not be avoided. The way to counteract the instability is to increase the electron beam rigidity, to make its motion during the collision smaller. Naturally it can be done using a strong longitudinal magnetic field in the interaction region. It is assumed that the Tevatron ring chromaticity can be made close to zero, so that the “weak head-tail” instability is negligible.

A peculiarity of the TMCI due to TEL is that the wake field has a skew force, for example, an originally horizontal displacement results in both horizontal and vertical displacements. Both direct and skew wakes are taken into account in this numerical simulation. The simulation reveals that, although the antiproton bunch motion is essentially two-dimensional (since the wake is 2D), the instability starts in that plane where the original lattice tune is closer to half integer, e.g. in the horizontal plane for the Tevatron ring. Multi-mode analysis, analytical consideration in two-particle model and numerical simulations of the TMCI due to electron beam in the Tevatron have all derived the threshold value of the magnetic field in the e-p interaction region:

$$B^{thr} \approx 17.5[kG] \frac{[N_{pbar} / 6e10] \cdot (\Delta v_e / 0.01)}{(\sigma_{pbar} / 0.7mm)^2 \cdot \sqrt{\frac{v_s}{0.001} \cdot \frac{|v_x - v_y|}{0.01}}} \quad (3.6.10)$$

Therefore, for nominal pbar beam parameters, the magnetic field in the interaction region should exceed 17.5 kG if the electron beam radius  $a$  is equal to pbar size of  $\sigma=0.7$  mm. That is the case of nonlinear BBC. For the linear BBC, the electron beam size is 2-3 times larger, the wake force is weaker for the same current density, and the magnetic field needed to control the TMCI is  $(a/\sigma)^2$  times lower. The operational field in the main solenoid of the TEL is about 35 kG, therefore we expect to see no problems due to transverse electron beam impedance.

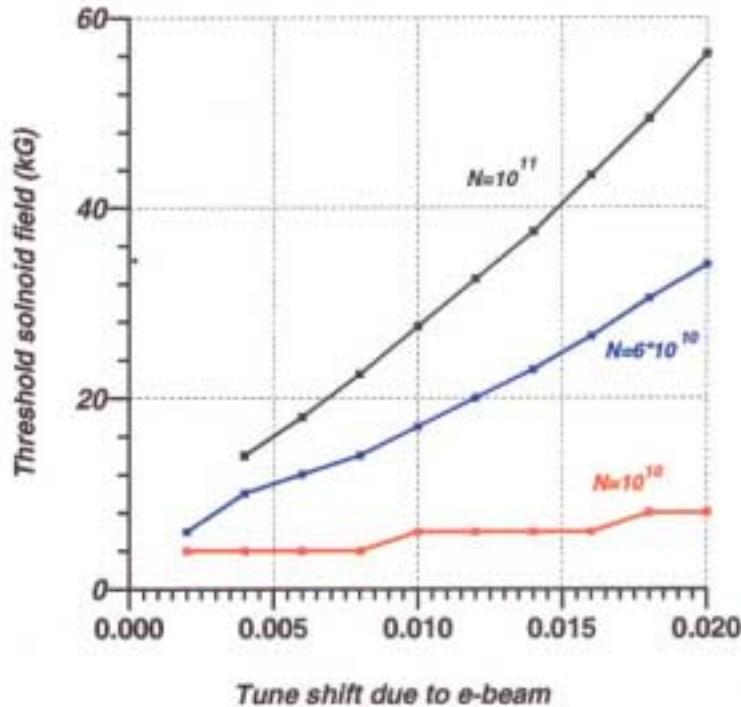


Figure 3.6.19 Threshold solenoidal field  $B_{thr}$  vs tuneshift due to electron beam at different pbar bunch populations  $N=(1,6,10) \cdot 10^{10}$ . Lattice tunes (0.585, 0.575), synchrotron tune 0.0012, rms pbar beam size  $\sigma=0.7$  mm.

### 3.6.3 Technical

Here we present technical aspects of the project, including the TEL magnetic system and its possible modification, the electron beam system for linear and non-linear BBC, diagnostics, and finally the operational issues and control.

#### 3.6.3.1 Magnetic System of the Tevatron Electron Lens

The magnetic system of the Tevatron Electron Lens (TEL) was manufactured by IHEP(Protvino) and tested at Fermilab. The system consists of seven superconducting and four conventional magnets and provides a solenoidal field to focus an electron beam. Low energy electrons follow the magnetic field lines from the cathode to the collector.

##### 3.6.3.1.1 Magnetic System of the TEL-1

The longitudinal cross-section of the TEL magnetic system is shown in

Figure 3.6.20. The system consists of seven superconducting (SC) magnets (one large solenoid plus six steering dipoles) and two conventional solenoid magnets each equipped with corrector coils. An electron gun is placed in center of the first conventional solenoid and an electron beam collector in the second one. The electron beam is born on the electron gun cathode, transported through the interaction region in the strong solenoidal field of the SC solenoid and absorbed in the collector. The requirement of the field quality is that the magnetic field lines in the main SC solenoid are straight within 0.2 mm in both vertical and horizontal planes along the 2-m length of the long dipoles.

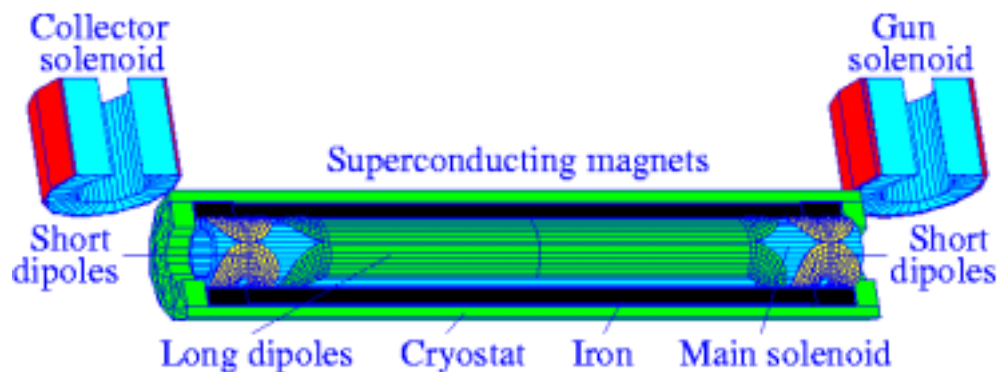


Figure 3.6.20 Longitudinal cross-section of magnetic system.

##### 3.6.3.1.1.1 Superconducting Magnets

The solenoid coil is constructed of a flat transposed cable consisting of 10 SC wires (NbTi filaments in copper matrix) each 0.85-mm diameter. The wire has 550 A critical current at 4.2 K and 5 T and Cu/SC ratio of 1.38. The dimensions of the bare cable are  $1.44 \times 4.64 \text{ mm}^2$ . Six steering dipoles are placed on the outer surface of SC solenoid coil. Four pairs of 250-mm long coils form (short) lateral vertical and horizontal dipoles at each end of the solenoid. Two pairs of 2-meter long coils are placed in the central region of the SC solenoid. All these dipoles are to correct the electron beam trajectory inside the magnetic system. The steering dipoles are wound of cable transposed from 8 wires of 0.3-mm diameter. The wire has 50 A critical current at 4.2 K and 5 T and Cu/SC ratio of 1.5. Dimensions of bare cable are  $0.45 \times 1.48 \text{ mm}^2$ . The lateral dipole cable

is made of SC wires only. The current in central dipoles is small, and the cable has three SC wires and five Cu wires. The central dipoles have one layer; lateral dipoles consist of two layers and an inter-layer spacer of 0.2-mm thickness.

Magnetic field calculations of the magnetic system were carried out using the MULTIC code. The SC solenoid coil together with steering dipoles is enclosed in a magnetic shield made of low-carbon steel. The shield is 48.5-mm thick over the length of 270 mm and 38.5-mm thick in the central part over 1.96-m length. The yoke reduces currents in steering coils, improves homogeneity of magnetic field inside solenoid aperture, compresses magnetic field lines at the ends of the coil block, and reduces stray fields. The winding of solenoid with preliminary tension and the compression of SC coil by the wrapping of the stainless steel half-shells, allows one to reduce degradation and training of the SC coil. The main parameters of the TEL SC magnets are presented in Table 3.6.3. Computer calculations of the solenoid coil stress have been performed for all stages of winding and showed that cable tension during coil winding have to be 200 N and preload higher than 1 MPa between coil and iron.

	Solenoid	Lateral	dipoles	Central	Dipoles
Field direction	Longitudinal	Horizontal	Vertical	Horizontal	Vertical
Inner coil radius, mm	76.00	100.0	103.7	100.0	103.7
Outer coil radius, mm	98.68	103.5	107.1	103.5	107.1
Coil length, mm	2500	270	270	1960	1960
Number of layers	14	2	2	1	1
Total turn number	7289	640	664	640	664
Operating current, A	1800	200	200	100	100
Central field, T	6.5	0.79	0.82	0.20	0.20
Maximal field in coil, T	6.5	2.2	2.2	0.5	0.5
Stored energy, kJ	950	1.2	1.3	0.9	1.1
Inductance, H	0.6	0.057	0.066	0.18	0.21
Critical current ( $B_{\max}$ , 4.6 K), A	3000	640	640	540	540
Critical temperature ( $B_{\max}$ , I), K	5.3	7.1	7.1	8	8

Table 3.6.3

All the SC coils and the magnetic shield are enclosed in a helium vessel. There is a box in the front of the helium vessel, which contains current leads, helium pipes and pipes going to a relief valve. The cold part of the magnetic system with mass of about 1350 kg is attached to the vacuum vessel in two cross-sections with the help of two vertical suspensions and two horizontal tension members in each of the cross-sections. The cold mass is fixed axially using longitudinal titanium tension members and the anchor is fixed to the vacuum vessel.

During the change of current through the SC solenoid dynamic heat release occurs in the coil and other metal parts. Some heat is due to hysteresis in magnetization of the superconductor and the steel of the yoke. Heat is also provoked by eddy currents generated in inner stainless pipe, in the copper matrix of SC wires and in the yoke. A

current ramp rate of less than 10 A/s is taken as a guideline, in order to limit the total heat load to liquid helium at 15 W.

#### **3.6.3.1.1.2 Quench Protection**

The SC solenoid coil is not self-protected against resistive transition and fast quench detection and removal of stored energy to the external dump resistor must be provided. A simulation of quench propagation through the coil was made for the case when quench was initiated at the end of the coil inner layer at the maximum current of 1800 A. The quenching lasts about 2 s. 90 % of the stored energy (about 1 MJ at 6.5 T) dissipates in the dump resistor and 10 % inside the cryostat, and the maximum temperature at the hottest point in the coil is about 270 K.

The energy stored in the SC dipoles is much smaller, about 1.3 kJ, and, in principle, one can allow all the energy to be dissipated in the coil if the quench is detected and the current is interrupted. In that case, the hot spot temperature will not exceed 120 K. However, to lower the risk of spreading the quench to the main solenoid, the scheme of quench protection with an external dump (as for the main solenoid) is also used in this case. The hot spot temperature does not exceed 43 K for lateral, and 29 K for central, dipoles.

Quench protection circuits for each SC coil compare the voltage across the coil with  $Ldi/dt$ . If the difference exceeds 1 V, a signal is sent to high current IGBT switches to disconnect the coil from power supply and to dump the coil current into the resistive load. Mechanical current breakers are installed in series with the solid state switches for redundancy.

#### **3.6.3.1.1.3 Conventional Magnets**

The gun and collector solenoids have almost identical design. Each is wound of  $8.25 \times 8.25 \text{ mm}^2$  Cu conductor with a 5.5-mm diameter water hole. The solenoid has a 0.4 T nominal magnetic field, 0.19-Ohm electrical resistance, and 18-mH inductance. The coil has 250-mm inner diameter, 474-mm outer diameter, and 300-mm length. The solenoid coil consists of 17 pancakes (total number of turns 391), which are assembled on a common pipe of a 240-mm inner diameter. Water temperature rise in the coil is  $30^\circ\text{C}$  at 0.7 MPa pressure drop and nominal current of 340 A. About 100 A of operating current are needed, in the short steering superconducting dipole, in order for the electron beam to be transported along the center of the warm solenoid.

Electron beam shape and position correctors are set inside each of the conventional solenoids. The corrector consists of four coils, which can be commutated either as a quadrupole or as two dipoles (vertical and horizontal). Each coil layer is shaped with  $0.74^\circ$  inner and  $40.04^\circ$  outer angles, 112.5-mm inner radius and 8.6-mm thickness. The length of coil is equal to 298 mm. The dipole field is equal to 19 G/A; the quadrupole field is equal to 6 G/A/cm.

#### **3.6.3.1.1.4 Results of Magnetic Measurements**

Magnetic fields in the TEL were measured by using 3D Hall probe and magnetic arrow set-ups. The latter was used only inside the main SC solenoid and operates with a

small trolley that holds a freely rotating magnetic rod. This trolley is moved inside the solenoid by means of a long track. A mirror is glued to the rod and, therefore, also rotates as the rod aligns itself with the local magnetic field. Beyond one end of the solenoid is a small laser aligned along the axis of the trolley's motion. The output beam hits the mirror and reflects back onto a position-sensitive device (PSD). Everything is adjusted so that, at the center of the solenoid, the laser beam is centered on the PSD. As the trolley is moved along the length of the solenoid, small deviations in the magnetic field appear as changes in the location of the reflected laser beam, which are detected by the PSD. The PSD produces signals that are easily converted back to horizontal and vertical displacement of the beam. Through geometry, the angle of the field is deduced, which is integrated to find the transverse displacement of the field along the length of the solenoid. A LabVIEW program automates the data collection and analysis process. The estimated errors of the spatial resolution are 10  $\mu\text{m}$  vertically and horizontally and 2 mm along the  $z$ -axis.

The ellipticity  $\varepsilon = 1 - B_y/B_x$  of the magnetic field in the solenoids was measured to be less than  $\pm 0.2\%$ , the accuracy of the measurement system. A corrector coil built into each solenoid can be configured as two dipoles (horizontal and vertical) with 19 G/A field strength of each or as a quadrupole with 6 G/cm/A strength. The corrector magnetic length,

$$L_m = \frac{1}{B_0} \int_{-\infty}^{\infty} B(0,0,z) dz = \frac{1}{G_0} \int_{-\infty}^{\infty} G(0,0,z) dz \quad (3.6.11)$$

was calculated to be 248 mm, making the integrated dipole field equal to 471.2 G-cm/A and the integrated quadrupole field equal to 148.8 G/A. This last value allows one to adjust the ellipticity by 10% at the maximum operating field of 0.4 T. The dipole correctors can rotate the field lines about  $\pm 1.3^\circ$  at the maximum field, which provides  $\pm 10$ -mm displacement of the field lines at the edges of the solenoid. The on-axis residual field along the magnetic axis is approximately 6 G near the iron cover and decreases linearly to about 2 G near the stainless steel cover.

In the first high-current test of the superconducting solenoid, 6.6 T was reached at the current ramp rate of 3 A/s and after that the solenoid could not be quenched up to 6.7 T at 10, 20, and 30 A/s. The magnet quenches very quietly and does not consume much helium at the quench. The typical operational field during Tevatron studies was about 3.5 T. The longitudinal distribution of the normalized field  $B/B_{\text{max}}$  is shown in Figure 3.6.21 for the superconducting magnets, where  $B_{\text{max}}$  is equal to 6.5 T in the solenoid (dashed line), 0.8 T in the short dipoles, and 0.2 T in the long dipoles (solid lines). The deviations of the magnetic axis from a straight line of the superconducting solenoid are shown in Figure 3.6.22. At full power, the vertical deviations are very small (roughly spanning  $-25$  to  $25 \mu\text{m}$  of the axis), while the horizontal deviations have more spread (from  $-100$  to  $75 \mu\text{m}$ ); however, these values are still less than the required 0.2 mm tolerance. The left side depicts how the field lines change from 3 T to 6 T, while the right side illustrates how five field lines, distributed horizontally, differ from each other. The deviations are small enough (about  $8 \mu\text{m}$  maximum, and the horizontal displacement shows similar uniformity) that unintentional lensing effects will be minimal.

### 3.6.3.1.1.5 Operational experience

The TEL has been installed in the Tevatron in February 2001, and been in operation since March and there were no quenches in the TEL at the typical operational field of 35 kG in the main solenoid. The magnetic system worked very reliably providing the control of the electron beam size and trajectory that allowed the first successful demonstration of the betatron tune shift of 980 GeV protons in the Tevatron. It was found experimentally that the electron beam can be steered to pass through the main solenoid if the gun solenoid field is in the range of  $B_{Gun}=1.9-4.2$  kG for  $B_m=35$ kG (outside the range, the beam touches parts of the vacuum system in the bend sections of the TEL).

### 3.6.3.1.2 Modifications of the Magnetic System for the TEL-2

Currently, we study possible modifications of the bending sections which can allow clean beam passage over even wider range of magnetic field ratios  $B_m/B_{Gun}$ . As it was mentioned above, that will make possible wider variation of the electron beam size in the main solenoid magnet.

Magnetic field simulations performed in the fall 2001 have shown that it is possible to increase magnetic field in the bend from 0.8 to about 2kG and increase the range of operational magnetic fields  $B_m/B_{Gun}$  about two fold if two conventional coils are installed and the bending angle is reduced from 90 degrees to about 45 degrees – see Figure 3.6.23.

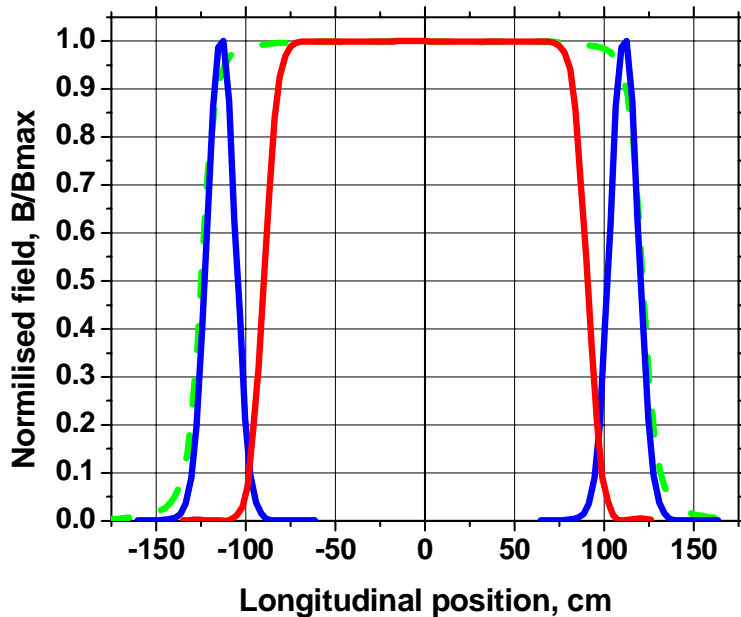


Figure 3.6.21 Longitudinal distribution of the normalized fields of the super-conducting magnets.

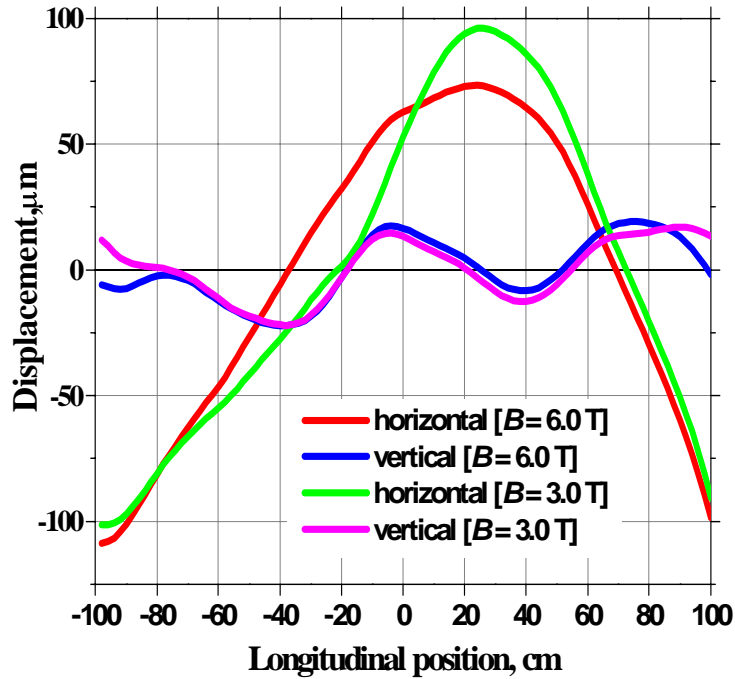


Figure 3.6.22 Transverse displacement of various field lines along the length of the main solenoid at different field strengths.

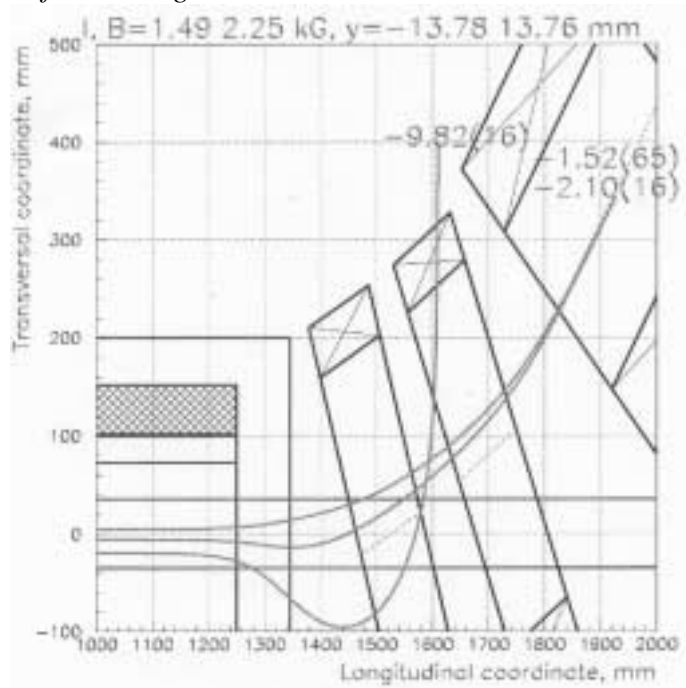


Figure 3.6.23 Magnetic field simulations for the TEL-2.

The new smoother bend also will also result in about 5 times smaller drift of the electron beam in the bend, and thus much weaker dependence of the vertical electron beam position on the electron beam current and energy. The 2<sup>nd</sup> TEL will be installed in A10 sector of the Tevatron ring and the closest cryo port will be some 15-30 ft away, so, corresponding modifications will need to be done in the cryogenic system design.

### 3.6.3.2 Electron Beam System of the TEL

The electron beam system of the TEL, which includes electron gun, collector, ion and secondary electron cleaning electrodes, high voltage modulator, vacuum system and beam diagnostics (BPMs, current monitors, scrapers, wire scanner). Results of the electron beam studies are presented.

#### 3.6.3.2.1 General Layout

Figure 3.6.24 shows the general layout of the TEL electron beam system. The total length of the TEL (flange-to-flange) is 3.65m; the interaction length (zone inside SC solenoid, where electron and antiproton beams can overlap) is about 2m.

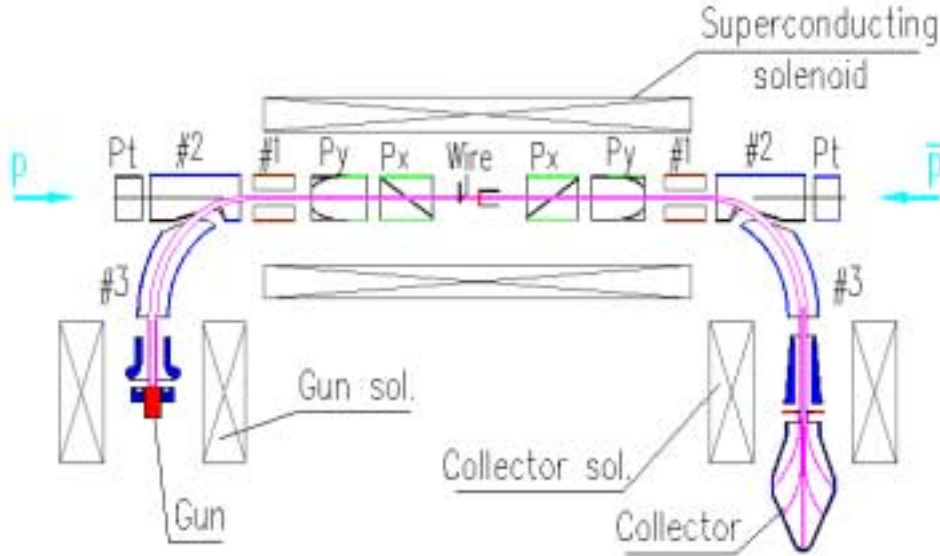


Figure 3.6.24 Electron beam system of the TEL.

The electron beam is born on the thermionic cathode of the gun immersed in some 4 kG magnetic field remains magnetized all the way to the collector.  $\Pi$ -shaped magnetic system is formed by two conventional and one super-conducting solenoids. The electron beam follows the magnetic force lines (magenta in Figure 3.6.24). Beam diameter in the main solenoid is defined by the cathode radius  $a_c=5\text{mm}$  and the ratio of the magnetic field at the cathode  $B_c$ , and in the main solenoid  $B$ :

$$a = a_c \sqrt{B_c / B} \quad (3.6.12)$$

The operational magnetic fields allow the electron beam size to be 3 times the antiproton rms size  $\sigma=0.5\text{mm}$ , while at the same time the electron beam does not touch any apertures. The typical TEL parameters are presented in Table 3.6.4.

electron beam energy,	$U_e$ , kV	6-12
maximum peak electron current	$J_e$ , A	2-3.5
magnetic field in main solenoid	$B_m$ , kG	35

in gun solenoid	$B_g$ , kG	3.7
e-beam radius in main solenoid	$a_e$ , mm	1.75
cathode radius	$a_c$ , mm	5
e-pulse width, FWHM	$\tau_e$ , mm	~800
repetition rate	$f_{rep}$ , kHz	47.7
current stability, peak-to-peak	$\Delta J_e/J_e$ , %	< 0.1
vacuum pressure	$e$ -8, Torr	2-8

Table 3.6.4 TEL operational parameters

The main SC solenoid has built-in dipole correctors for electron beam position and angle steering. Additional 4 coils are built-in in the gun and collector solenoids and can be used as quadrupole correctors of the beam ellipticity

The beam diagnostics consist of two pairs ( $P_x$ & $P_y$ ) of pick-ups (BPMs) 150mm long and  $\varnothing 70$ mm each, located at the beginning and at the end of the interaction zone. Pick-ups made of diagonally cut SS cylinder for better linearity. BPMs can measure positions of electron, proton and antiproton beams. Gun and collector beam currents as well as beam losses on the scraper electrode at the collector entrance are measured by inductive coils (IC). Two wires can be remotely introduced into the center of the lens for the beam profile measurements in both (X&Y) planes.

Figure 3.6.25 shows the TEL electrical circuit. Vacuum beam pipe and pick-up electronics stay at the ground potential. Cathode and anode potentials are negative, typically -10kV to -15kV and held by low-current DC power supply (V1) to compensate beam losses to the ground. High-current power supply (V2) with potential up-to +10kV drives cathode to anode beam current. To modulate the beam current three different types of HV modulators were used. The modulating positive signal feeds the electron gun anode through a capacitor.

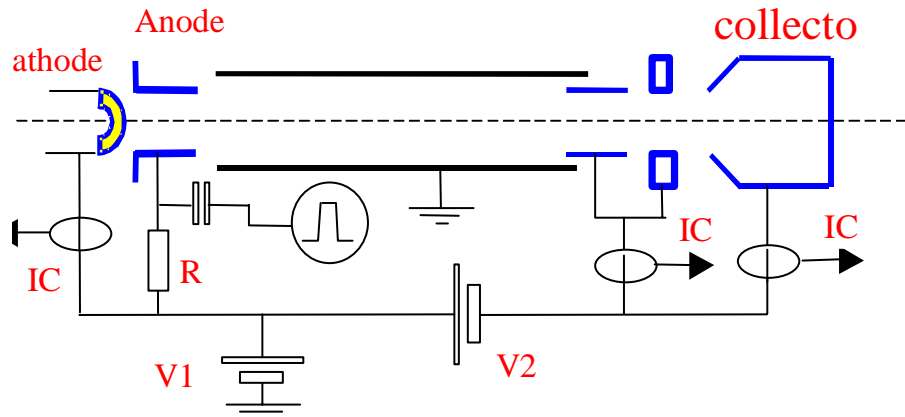


Figure 3.6.25 Electrical circuit of TEL.

The electron beam ionizes residual gas and if these ions and electrons are trapped and stored, their charge may change the lens performance. For cleaning the ions and electrons, several HV cleaning electrodes are installed. Two of them (#1) are installed inside the main solenoid, each consist of a tube ( $\varnothing 70 \times 129$ mm) cut in half and these two halves are insulated by semi-conducting glass. Ions can escape if cleaning potential ( $\pm U$ ) strongly distorts the potential well due to the electron beam space charge. Semi-

conducting glass avoid storing of the secondary electrons as well. Two elbow electrodes (#3) in the bends work the same way. The electron beam size at that place is about 15-20mm, hence  $\pm(5\text{kV to } 8 \text{ kV})$  of voltage thought to be enough for the cleaning. Cylindrical electrodes (#2) provide ion cleaning in longitudinal direction by changing potential barrier. The cleaning procedure for the TEL is not studied well yet.

### 3.6.3.2.2 High-perveance Electron Gun

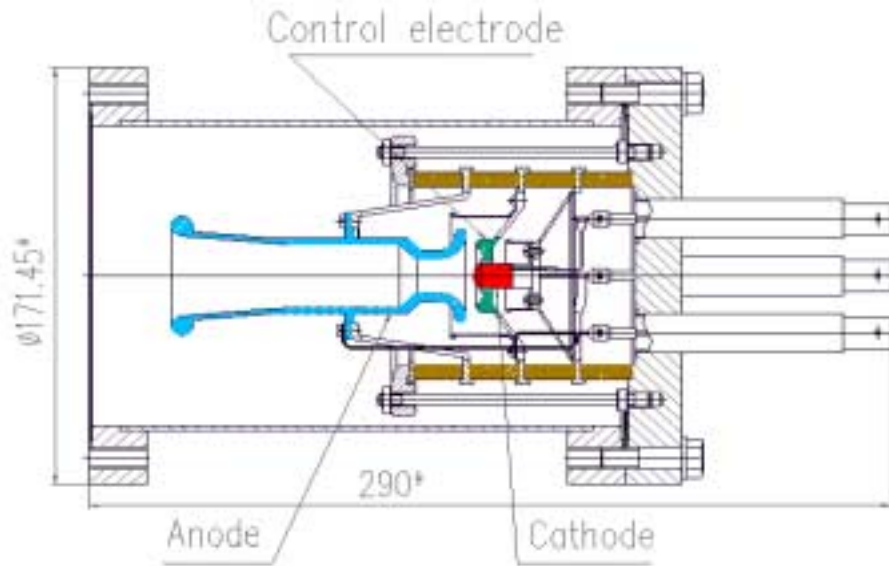


Figure 3.6.26 Electron gun for TEL.

The electron gun, see Figure 3.6.26, employs a 10 mm diameter convex cathode and can provide 10A of pulsed current and about 3A DC. The measured perveance of the gun is  $5.6\mu\text{A}/\text{V}^{3/2}$ , which is close to the design value<sup>46</sup>. The gun is assembled on 6.75" CF flange. All the electrodes are insulated by 4 ceramic rings (ID×OD=79×85mm and 20mm wide) and are constricted by stubs. The electrode capacitances are: 40pF anode to ground, 38pF anode to control electrode, 17pF anode to cathode. Vacuum HV feed-throughs provide 20 kV DC to all electrodes. In presence of a magnetic field the maximum electric potential may fall to 15kV if the vacuum is worse than  $5 \times 10^{-7}$  Torr; this is due to Penning discharge. We plan to fix this problem in the improved gun design.

In the pulsed regime, the anode is driven by a pulse modulator. In the first tests a tetrode modulator with 800 ns and up to 7.5kV output pulse amplitude was used. The plot of beam current vs. anode pulse voltage for 50 Hz and 50kHz (operational regime) repetition rates is shown in Figure 3.6.27.

The difference in behavior between low and high repetition rate can be explained by the presence of stored ions in the case of 50kHz. During the  $20\mu\text{s}$  between electron pulses, the ions have not enough time to escape from the TEL and partly compensate the electron space charge. In this case, the beam current follows Child's law. In absence of ions we have some restriction of electron current due to the beam pipe perveance.

For the electron beam profile measurement, two wire scanners are installed in the TEL close to the middle plane of the main solenoid. One is for horizontal plane and the other

is for vertical plane. Wires can be moved in or out of the beam pipe by remotely controlled step motor. In normal operation with the proton beam they are moved completely out of the beam orbit in order not to disturb the proton beam or/and not to burn out the wire. The geometry of the wire is shaped like a “fork”. The distance between the fork claws is 15mm, from the wire to top edge 22mm, wire diameter 100 $\mu$ m, the tube diameter 70mm. As an ancillary benefit, the dimensions give us a good scale for calibration of steering strength of correctors for the electron beam and in turn, to calibrate the pick-up BPM systems.

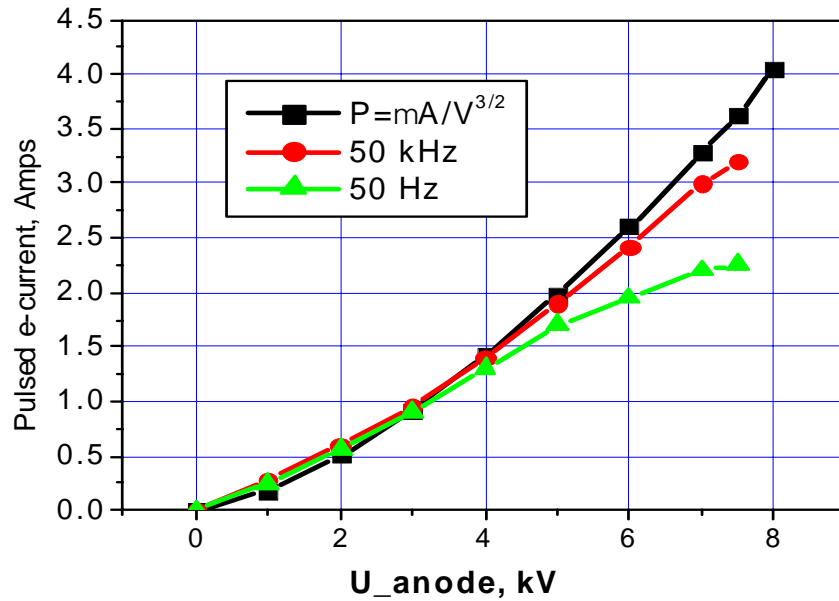


Figure 3.6.27 Beam current vs. anode voltage at 50Hz and 50kHz

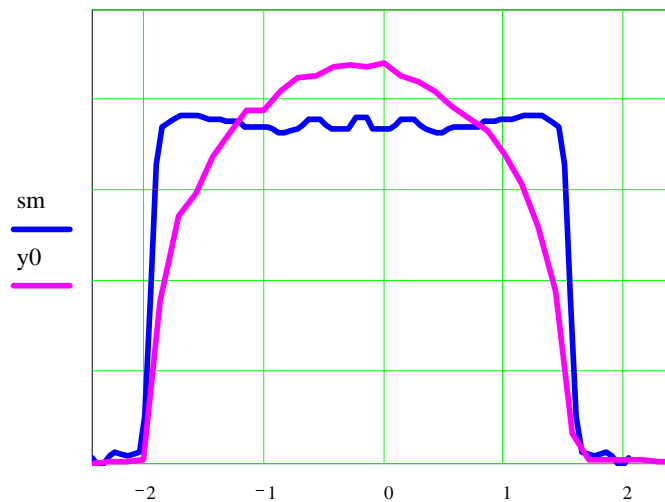


Figure 3.6.28 Electron beam current density profile.

Measured (X-slices) and restored beam profiles are shown on Figure 3.6.28 (top). The beam diameter is about 3.5 mm. The restored profile is in a good agreement with the

two-dimensional electron current profile (bottom), previously measured by special beam profile-meter at the TEL prototype. That profile-meter measured a small portion of the beam current, which goes through tiny hole in electron collector. By scanning the electron beam in XY plane we can measure the 2-D electron current profile. The electron current density profile is almost flat as required for the linear beam-beam compensation, but can be changed by applying negative potential to a special (control or “profiler”) electrode near the cathode. In this case the beam profile becomes smoother, while it reduces the total current and the beam size decrease.

### ***3.6.3.2.3 Electron Gun for Non-Linear BBC***

An electron beam with transverse charge distribution close to the Gaussian is thought to be needed for non-linear beam-beam compensation. No studies have been done so far in that direction. Nevertheless, we currently investigate the electron gun geometry for non-flat current profiles. In particular, according to numerical tracking results (see above) a “smooth edge” distribution is anticipated to be beneficial for the linear beam-beam compensation as the high-order resonance strengths will be suppressed compared to a flat electron current density profile. Figure 3.6.29 shows electron current distributions for current electron gun geometry (black curve) and for modified geometries; all were calculated using the SuperSAM code. The corresponding shapes of the electrodes are shown in Figure 3.6.30.

### ***3.6.3.2.4 HV Modulator for the Electron Gun***

The HV modulator uses the output from the anode of a grid driven tetrode. The tube anode is connected to a +10kV dc anode supply through a 1500 $\Omega$  resistor. The modulating voltage on the anode of the tetrode is then ac-coupled through two 1000pF ceramic capacitors to the electron gun anode. This modulator has the advantage that it is not susceptible to radiation damage and can be installed directly adjacent to the Tevatron beamline.

A CPI/EIMAC 4cw25000B water-cooled tetrode, with a maximum plate dissipation of 25kW, is used in this modulator. Its anode voltage is supplied by a Hipotronics 10kV,16A, dc power supply. An additional LC filter (1.5H, 20 $\mu$ F) was added to the output of the Hipotronics supply to reduce ripple to less than 1 part in 10,000. The anode supply is connected to the tetrode through a 1500 $\Omega$ , 250kW, water cooled resistor (Altronic Research). The grid of the tetrode is driven by an Amplifier Research 500A100 amplifier which can provide 500 watts of power from 10kHz to 100MHz.

To compensate a single bunch of protons or antiprotons, the tube is typically operated with a screen voltage of 750V and a dc grid voltage of -15V. Under these conditions, the voltage on the anode is held slightly above the screen voltage at 1kV with a plate current of 6A. The tetrode grid is then pulsed with a negative voltage pulse from the broadband amplifier, reducing the current flow through the tetrode. The positive pulse appearing on the anode is then coupled, using two 1000pF ceramic capacitors in parallel, through a short (0.6m) section of 50 $\Omega$ , RG213 cable to the anode electrode of the electron gun. A typical output pulse is shown in

Figure 3.6.31.

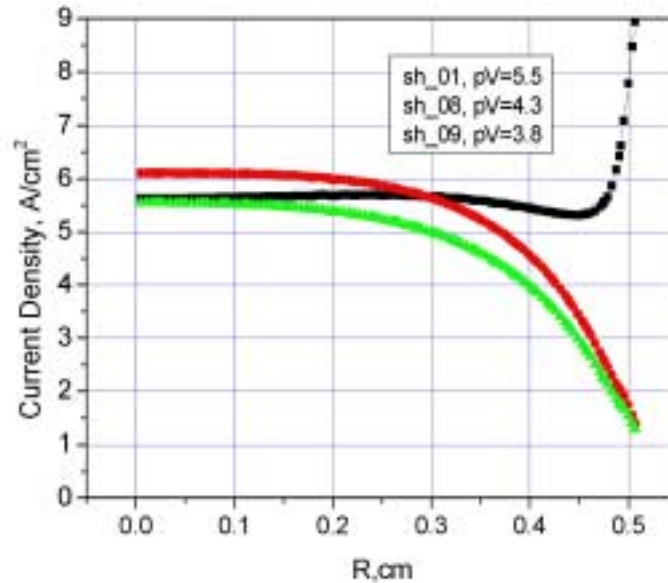


Figure 3.6.29 Calculated distribution of electron current density vs radius with original (black) and modified geometry of the gun electrodes (green and red)

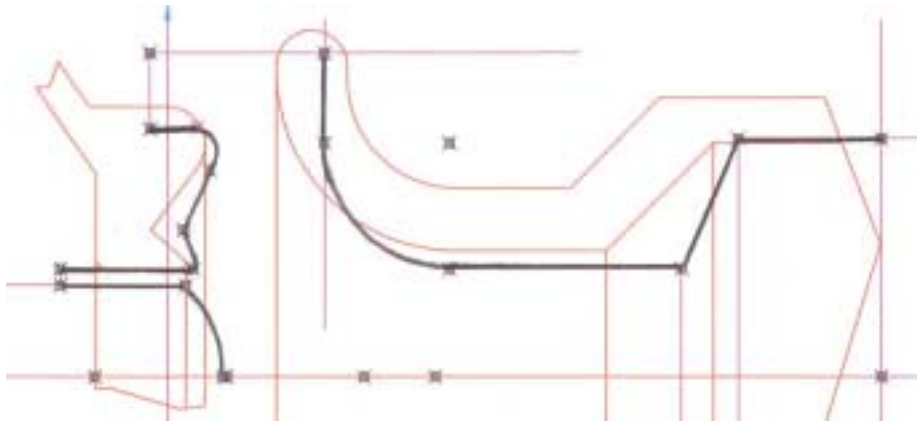


Figure 3.6.30 Shapes of electron gun electrodes (anode, cathode and near-cathode electrode) for bell-shape profile (black) and for flat-top electron current profile (red line).

Since the gun anode must be charged through the  $1500\Omega$  resistor, the risetime is limited by the sum of the tetrode's anode-screen capacitance (35pF), the capacitance of the cable connecting the modulator to the gun (60 pF), and the gun anode to ground capacitance (60pF). A pulse to pulse amplitude stability of 2 parts in ten thousand was achieved by applying a feedforward compensation signal to the grid of the tetrode to reduce ripple on the modulator output at power line frequencies.

There is need for a higher amplitude HV pulse (some 12-14kV) for linear BBC operation. That would require different HV DC power supply and little modification of the circuitry. Two HV modulators will be necessary for two TELs and one more spare for routine operation.

The second modulator tested was 20kV, 50ns wide pulser (model # FPG20-50S) designed and manufactured by FID Technology. The pulser uses a combination of fast

(<1ns) closing Fast Ionization Device (FID) switches and fast opening Drift Recovery Diodes (DRD) to generate the output pulses. The pulser is arranged into four identical blocks whose outputs are then combined. Each block has a single DRD shunting its output connector. The DRD is connected by coaxial cables to two LC circuits, each LC circuit having its own stack of FID switches. The pulsing sequence begins when one of the two FID stacks closes, exciting the first LC circuit and sending current through the conducting DRD. After a half cycle oscillation in the first LC circuit, the current reversed direction and the second FID stack closes, exciting the second LC circuit. During this time charge is being pumped out of the DRD. When all of the charge has been pumped out, the DRD opens, interrupting the large current flow and generating a 5kV, 50ns pulse at the output.

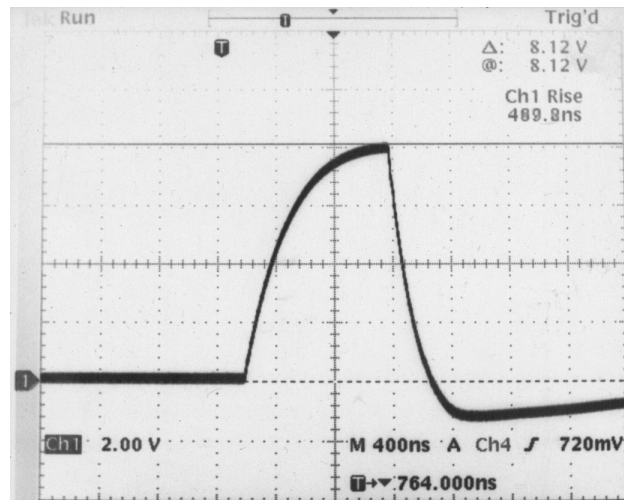


Figure 3.6.31 *Tetrode modulator output pulse (2kV/div) with a sweep time of 400ns/div.*

The four 5kV block outputs are combined, using a Blumlein type circuit consisting of four, 6m long, 100 $\Omega$  coaxial cables, into a single 20kV positive pulse. The output is matched into a 480 $\Omega$  resistive load. The pulse width is fixed at 50ns and the pulse height is adjustable from 0-20kV by varying the 0-300V dc input voltage. The pulse repetition rate is limited to 50kHz at the maximum voltage due to component heating.

Since the output consists of positive pulses referenced to ground and the electron gun anode is normally biased at the negative cathode potential (-13kV), the pulser output must be capacitively coupled to the gun anode through a 3300pF, 30kV, ceramic capacitor. The pulser, along with its combining network, 480 $\Omega$  resistive load (water and air cooled), and output coupling capacitor is enclosed in a shielded equipment rack to eliminate electrical noise generated in the combining network from interfering with other electronics in the TEL. We have experienced several failures of the HV connectors on the cable between the modulator and the electron gun anode feedthrough due to corona discharges at voltages above 15kV.

### 3.6.3.3 Diagnostics and Operation

#### 3.6.3.3.1 Introduction

The 1<sup>st</sup> TEL operation requires(in order of urgency): better electron beam steering, better proton beam diagnostics, and a better quality electron beam. To achieve more precise steering, we are currently working on the BPM hardware and electronics improvement (the existing ones gave unreliable readings of the proton bunch position).

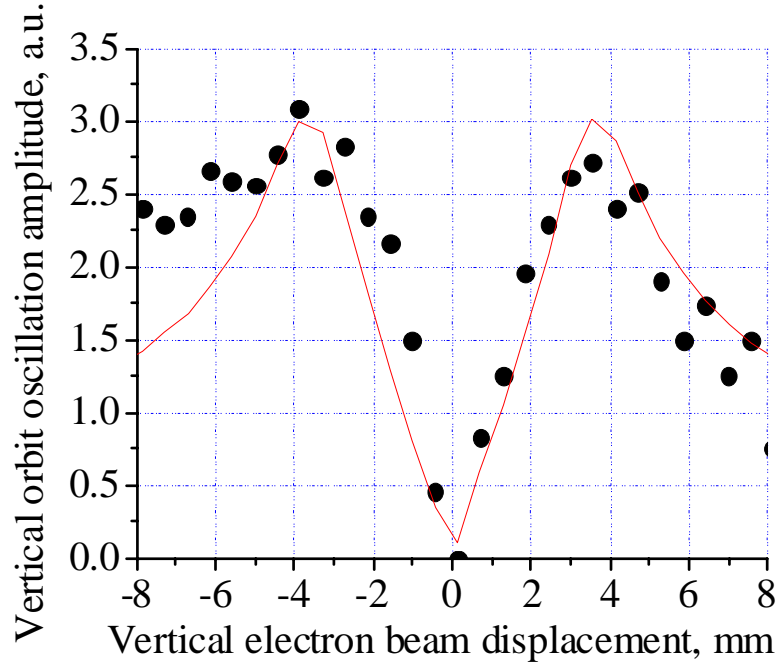


Figure 3.6.32 *Rms amplitude of vertical proton orbit variation vs vertical position of AC electron beam.*

Using “tickling” of the proton orbit with the electron beam can potentially improve the steering as well. The idea is similar to the “K-modulation” in the beam based alignment: variation of the electron current in the electron lens should cause variations in the proton beam orbit around the ring if the electron lens beam is not centered. Figure 3.6.32 shows the rms amplitude of the vertical proton orbit variation at the Tevatron BPM located at A0 sector vs vertical displacement of the electron beam at F48 which had the current modulation of  $J_e = 1.02 + 0.18\sin(2\pi \cdot 107\text{Hz})$  A. The amplitude becomes equal to 0 if the proton beam goes through the center of the electron beam. The 7 mm distance between the two peaks reflects an effective diameter of the electron current distribution, and, thus, indicates angular misalignment of the electron beam because it exceeds the electron beam diameter of about 3.5 mm. Therefore, steering by the orbit tickling should concentrate not only on the search of the minimum orbit response, but also on having two maxima closer to each other. In the first experiments, such a tickling measurements took about 2-3 hours, and now we are looking for a faster automated system.

### 3.6.3.3.2 Proton and Antiproton Beam Diagnostics

Besides the BPM system of the TEL, we also use the beam diagnostics of the Tevatron to monitor proton and antiproton parameter, which include intensity, emittance, orbit, lifetime and tune. The Tevatron orbit measurement system has a resolution of 150 micrometer. The tunes are measured by the Shottky spectra analyser. A new bunch-by-bunch tune meter is under commissioning. Its resolution needs to be improved to be better than 0.001. The beam emittances are measured by the flying wire systems. We found that the flying wire system gives large errors, e.g., about 14% in horizontal proton emittance. We expect that recently installed synchrotron light monitor will perform better and will allow us to monitor the proton or antiproton emittance variations during the beam-beam compensation studies. The beam lifetime is monitored by the Fast Beam Integrator (FBI), which relies on the wall current monitor. We will also be able to monitor the luminosity and the proton losses bunch-by-bunch, which is supplied by the D0 and CDF detector via ACNet. And we also can ‘tickle’ the proton or antiproton beam orbit by modulating the electron beam current. That method provides us the information for precise centering of the electron beam onto the proton (or antiproton) beam.

We also look forward to having more reliable proton diagnostics for the emittance measurements (e.g., synchrotron light system instead of flying wires) and an automated tune measurement system for the multi-bunch measurements. Currently, Tevatron beam diagnostics is unable to provide reliable data on p/pbar size and tune on bunch-by-bunch basis with needed accuracy.

### 3.6.4 Project Plan

Table below summarizes implementation plan of the Beam-Beam Compensation project from November 2001 until March 2006. Columns “Current configuration”, “Linear BBC” and “Non-linear BBC” refer to Run IIa conditions (36x36 bunches); “Nonlinear BBC→ Zero Crossing Angle” refers to Run IIb with 132 ns bunch spacing.

	Current configuration		Linear BBC (2 TELs)		Nonlinear BBC		Nonlinear→ ZeroX-angle	
	Exist	0	the 2 <sup>nd</sup> set of magnets, minor changes in design, magnetic measurements, radiation protection – 11mos	330 k\$	Use existing	0	Use existing (TBD – larger e-current and smaller diameter may require new magnets)	0
Power Supplies	exist, minor improvement	0	2 <sup>nd</sup> set of PSSs	70k\$	Use existing	0	Use existing	0
Quench protection	Exist	0	2 <sup>nd</sup> set of QPS	60k\$	Use existing	0	Use existing	0
Electron gun	Exist, design and R&D under way to increase current to 5-7A and voltage to 30kV	40 k\$	2 more copies of the improved design gun	70k\$	Optimized shape gun electrodes	25k\$	3 optimized shape electrode guns with 3-5 time larger current and twice larger cathode	100 k\$
Electron collector	Exist	0	two the same type	60k\$	Use existing	0	3 100kW collectors	150\$
HV PSs for e-system	Exist	0	one more set of PSSs	40k\$	Use existing	0	Higher current higher voltage	120 k\$
HV pulse generator and its PSs	Exist	0	build two somewhat modified tetrode 12kV 2MHz pulsers	300 k\$	Use existing	0	Two 18kV and 6MHz pulsers to be built, existing	100 k\$

							20kV PSs	
Vacuum/diagnostics	Exist	0	Build the 2 <sup>nd</sup> set	60k\$	Use existing	0	Use existing	0
Cables/LCW/construction	Exist	0	Work at sector A10	150 k\$	Use existing	0	Additional cable work	60k\$
Cryo	Exist	0	He/N2 connections, bypass modification	70k\$	Use existing	0	Use existing	0
Studies	14TeV shifts till May'02	0	Magn.meas.+tests in E4R (3mos), then 30 Tevatron shifts	40k\$	30 Tevatron shifts, DC wires	95 k\$	e-Studies in E4R with SC magnets needed (6 mos)	300 k\$
Theory/calculations <sup>1</sup>	None		1S+1RA		1S+1RA		1S+1RA	
Cost <sup>2</sup> , M&S	total in FY'01-02	40k\$	50%-50% in FY'02-03	1500 k\$	All in FY'04	150 k\$	2/3 in FY'05 1/3 in FY'06	1000 k\$
Time scale	now-June'02		2yrs till Oct'03		1yr - Oct'04		1½ yr till Mar'06	
Additional man-power <sup>3</sup>	None		2x(P,EE),1x(S,PE,ME, CS,D)		2P, 1S		2x(P,EE),1(S,ME)	

<sup>1</sup> in terms of people working on the project: S – Scientist or Ass.Sci., RA – postdoc

<sup>2</sup> 20% contingency added

<sup>3</sup> compared to Summer-Fall'01 work-force of 2 Physicists (P), 1 Student(S) and 1ProjectEngineer(PE); abbreviations: EE-Electrical Engineer, ME-mechanical engineer; CS – computer specialist; D- drafter; assumed that the people requested work over the time period listed in each column

### 3.6.4.1 Status as of November, 2001

Fermilab Beams Division BBC (Beam-Beam Compensation) Project group is currently focused on implementation of the *linear BBC*. One TEL was designed, built, tested, installed in the Tevatron Sector F48 and operated by March 1, 2001. Because of the larger horizontal beta function  $\beta_x=101\text{m} \gg \beta_y=29\text{m}$  at that location, the first TEL can shift mostly horizontal tune of the Tevatron beams. It is anticipated that the second TEL to be built will be installed at the Sector A10 where  $\beta_y=172\text{m} \gg \beta_x=56\text{m}$  will shift mostly the vertical betatron tune.

In the period March-October 2001, the TEL operated in a single bunch regime with 47.7 kHz electron pulse repetition rate. The maximum horizontal tuneshift achieved with 980 GeV protons (6 shift of studies) is about  $dQ_x=+0.0071$  with 980 GeV protons, while vertical tune shift is about 4 times less, all in a good agreement with theoretical expectations. Among other achievements we note: a) a decent proton beam lifetime exceeding 20 hrs has been obtained with maximum electron current; b) it has been demonstrated that electron beam separated by 5 mm from the proton beam, the default regime for the BBC, as the electron beam will collide with pbars, does not affect the proton beam (infinite lifetime); c) it has been demonstrated that having TEL magnets on and/or electron beam but not interacting with the Tevatron beams does not affect the Tevatron beams. That is, no significant changes in orbits, tunes, coupling, chromaticity, dispersion, lifetime, or impedance are seen.

A Fermilab Beams Division Internal Review of the BBC project took place on June 4, 2001. Status of the project was appraised positively, and recommendation to continue the studies has been given. For that it was decided to allocate about 3 Tevatron study shifts a month for the BBC in order to finish studies early in 2002. This is, of course contingent on the collider meeting certain operating performance criteria.

### 3.6.4.2 Plans for FY 2002

Further plans of the BBC project in FY02 include beam studies and the start of construction of the second TEL, and preliminary studies of non-linear beam-beam compensation.

Tevatron beam studies with the TEL are focused on demonstration of single electron lens operation to produce tuneshift of about 0.005-0.01 on a single antiproton bunch at collision (980 GeV) without significant degradation of the luminosity lifetime.

The beam studies plan includes:

- a) operation with 980 GeV antiprotons;
- b) investigation of the dependence of the p(pbar) lifetime on e-beam steering, current, size and shape, magnetic field, current and position stability, p(pbar) size/emittance;
- c) understanding of the ion accumulation process and relevant effects, clearing/storing of ions;
- d) measurement of the p(pbar) emittance evolution under impact of the TEL;
- e) attempting improvement dynamics of a single pbar bunch by the only existing TEL;
- f) studies of non-linear effects under operational conditions similar to those required by the *non-linear BBC*;
- g) observation of “strong head-tail” instability at reduced main solenoid magnetic field.

In parallel, we will continue hardware improvement, e.g., of the electron gun, electron and p(pbar) beam-position monitors, electron beam diagnostics, power supply stabilization, and higher power HV modulators.

Building the second TEL will require:

- a) studies of the bending section magnetic field optimization and potential design changes in positioning gun and collector solenoid magnets
- b) design of the magnetic structure for the 2<sup>nd</sup> TEL
- c) design of cryogenic system for the 2<sup>nd</sup> TEL
- d) measurements of the radiation levels at A10
- e) calculation/design of radiation shielding for the 2<sup>nd</sup> TEL
- f) fabrication of the magnetic system and quench protection system for SC magnets
- g) design and build modified 30 kV electron gun, build electron collector, electron beam diagnostics and vacuum system
- h) design and fabrication of a faster HV modulator for Run IIb operation;
- i) assembly and test of the TEL in E4R building
- j) preparation work at A10 sector, including radiation shielding for SC magnets and cryogenics infrastructure
- k) installation and commissioning of the second TEL
- l) modification of the control system.

We plan to accomplish items a) to e), and part of item g) (design of 30 kV electron gun) in FY2002. Items f) to h) are to be started in FY2002 and finished in FY2003.

In parallel, we will fabricate and test the electron gun for non-linear beam-beam compensation and perform analytical studies and tracking of the Tevatron beam dynamics with non-linear BBC devices.

### **3.6.4.3 Plans for FY 2003**

The plan for FY03 includes finishing fabrication of the second TEL, its installation and commissioning of the system of two TELs for linear BBC; design and fabrication of the electron gun for the nonlinear beam-beam compensation; non-linear BBC experiments with Tevatron beams.

To complete the system of two TELs for linear beam-beam compensation in FY03 we plan : a) fabrication of the magnetic system and quench protection system for SC magnets; b) fabrication of electron collector, electron beam diagnostics and vacuum system; c) fabrication of faster HV modulator; d) assembly and test of the 2<sup>nd</sup> TEL in E4R building; e) preparation work at A10 sector, including installation of radiation shielding for SC magnets and cryogenics infrastructure; f) installation and commissioning of the second TEL; j) modification of the control system.

In parallel, we will perform Tevatron beam studies with non-linear electron beam profiles to better understand beam dynamics issues of non-linear BBC.

### **3.6.4.4 Manpower**

Currently, the BBC group has only enough man power to perform beam studies and make minor hardware/software improvements. More man power will be needed as soon as we start design, fabrication and test of the second electron lens, design and test of the electron beam system for non-linear BBC.

We anticipate either new hires or transfer of people to the group or temporary assignments from other BD departments. In particular, we need (FTE in FY2002):

- 1 Electrical Engineer and 1 Tech to fabricate/test QPS
- 1 Electrical Engineer and ½ Tech to develop HV modulator
- 1 Electrical Engineer and ½ Tech to develop other HV PSs
- 1 Electrical Engineer to build beam diagnostics
- 1 Mech.Engineer – project engineer
- 1 Drafter
- ½ CryoEngineer
- ½ Computer Specialist
- 1 Scientist (Assoc.Sci. or higher) to carry out electron gun/collector diagnostic development/fabrication/test .
- 1(or 2) Scientist(s) (grad student/RA) to take part in beam studies
- 2 Scientists to carry out analytical and numerical studies of nonlinear BBC.

In addition to that we expect to get some help from external organizations and collaborators, including IHEP(Protvino, Russia), which will take part in design and fabrication of the magnetic system for the 2<sup>nd</sup> TEL, and Budker INP (Novosibirsk, Russia), which helps us to perform Tevatron beam dynamics simulations and computer tracking.